



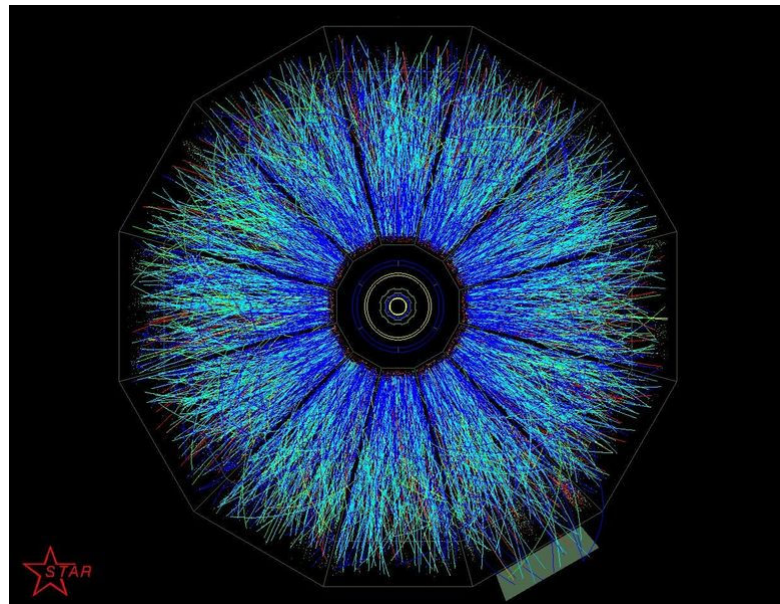
UNIVERSITY OF TURKU

Radiation and particle detectors

UFYS3054

Lecture Notes

Edwin Kukk



University of Turku

2011

Literature:

- Konrad Kleinknecht: Detectors For Particle Radiation (Cambridge Univ. Press 2003)
- Dan Green: Physics of Particle Detectors (Cambridge Univ. Press 2005)
- Marcel Miglierini: Detectors of Radiation (Lecture Notes, Slovak Univ. of Technology)
- B. Van Zeghbroeck: Principles of Semiconductor Devices, 2004

Cover picture:

Particles erupt from the collision point of two relativistic (100 GeV) gold ions in the STAR detector of the Relativistic Heavy Ion Collider. Electrically charged particles are discernible by the curves they trace in the detector's magnetic field. *Image source: RHIC.*

1 Introduction

The purpose of this short course is to cover a range of principles and actual devices used to detect photons and ionized particles. The variety of the detectable particles is very large, and the scope of the course must restrict it in some ways.

Radiation:

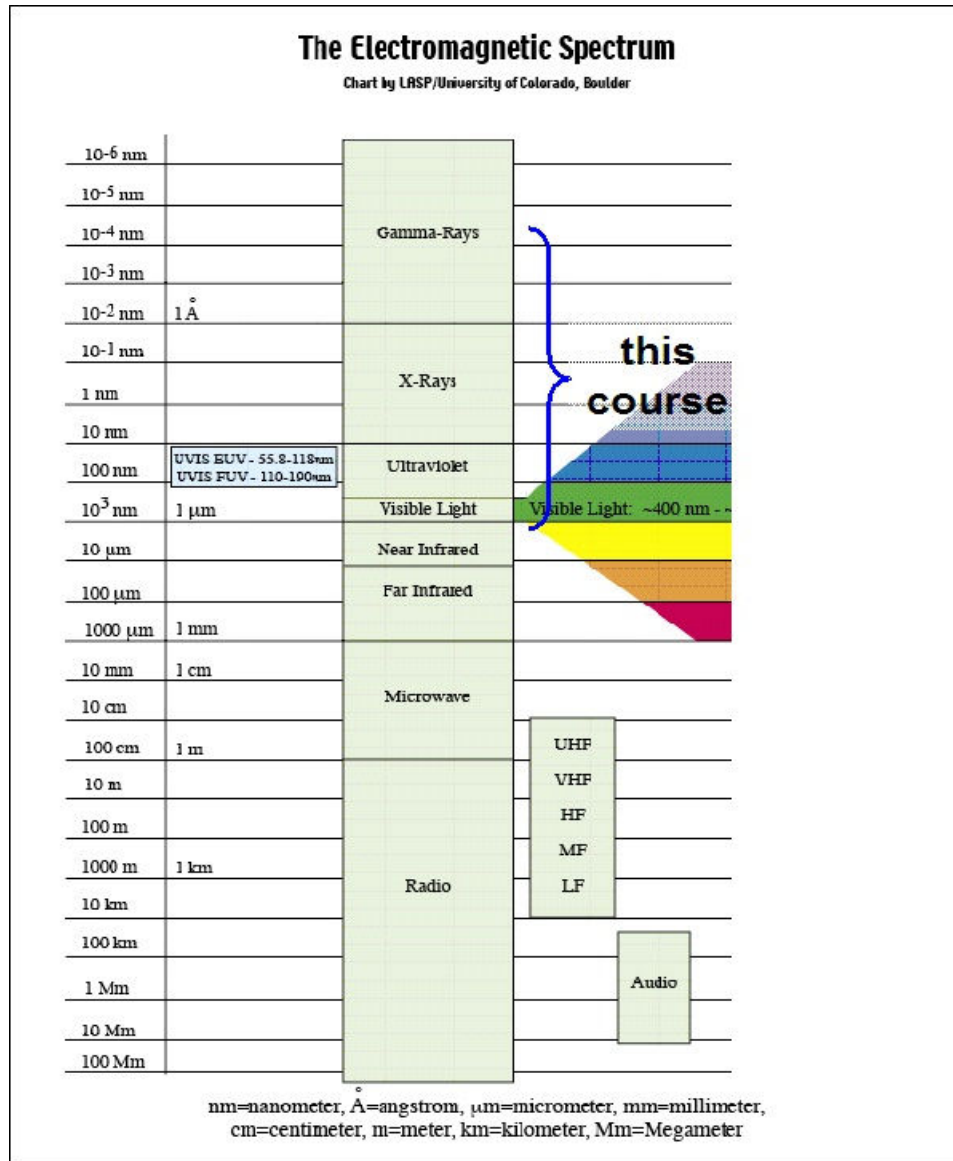


Figure 1. The part of electromagnetic spectrum covered by this course.

The term of “radiation detector” is taken here in a rather general sense, covering also devices such as solar cells.

Particles:

- Charged particles
 - electrons
 - ions
- Neutrons

Why many different detectors?

- Each region of the electromagnetic spectrum requires different detection methods
- Large range of particle masses: light (e^-) and heavy ions (atomic, clusters with $M > 1000$ atoms).
- Measuring different properties:
 - Flux of particles
 - Energy dose
 - Number of individual particles
 - Energy or wavelength of single particles
 - Velocity (momentum) of single particles
 - mass and/or charge of particles
 - position and/or time resolved detection

Firstly, a physical background common to all detectors covered here is presented. Then some general aspects of particle and radiation detection – units, terminology etc – are presented. Next, for different types of detectors, the physical foundations of their operation is covered, followed by their practical design examples. Also the basics of electronic circuits and signal treatment is given.

2 Interaction of particles and radiation with matter

From the viewpoint of particle detection, it is in general necessary to release a certain quantity of electric charge Q in the detecting medium, that can then be collected and processed. From the processes described below, these creating freely movable (vacuum or conduction band) electrons and ions (gas) or holes (solid) are of interest.

2.1 Radiation

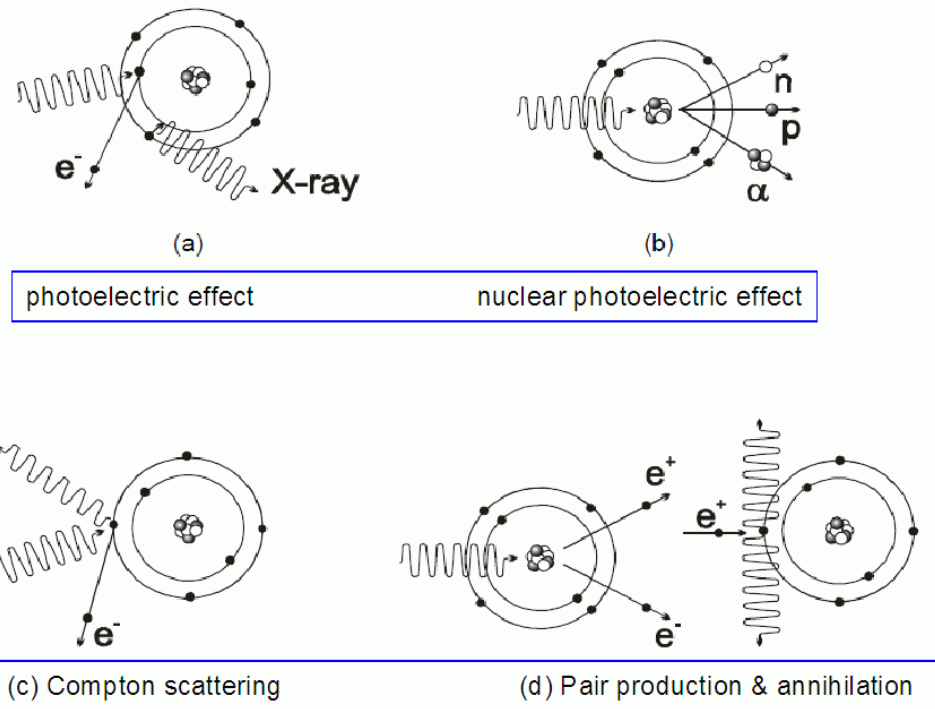


Figure 2. Interaction of radiation with matter [M. Miglierini].

In the energy range from visible light to g-rays, then following processes are the main forms of interaction between the photons and matter:

2.1.1 Photoelectric effect

A photon interacts with a bound electron in an atomic or molecular orbital or in an energy band of a solid (Figure 2a):



The photoelectric effect thus creates free electrons that can be collected using electric fields and handled by electronic circuits. It is the basis of many radiation detectors and ought to be studied more closely. In atomic photoemission the departing photoelectron obtains the kinetic energy

$$E_k = h\nu - E_b(nl), \quad (1-2)$$

where $E_b(nl)$ is the binding energy of electrons in the atomic orbital with the quantum numbers nl . The lowest energy of the radiation that can cause photoemission in atoms is thus

$$h\nu_{\min} = I(A), \quad (1-3)$$

where I is the **ionization energy** (the binding energy of the outermost electron shell) of the element A. As seen from Figure 3, it varies greatly, being smallest for the alkali metals and highest for rare gas atoms.

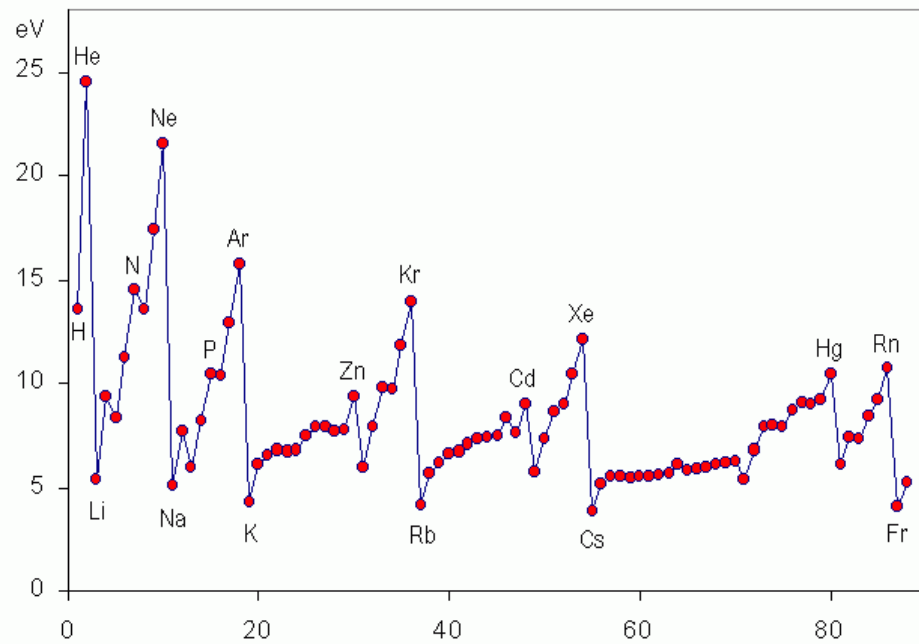


Figure 3. Ionization energies of free atoms.

In solids, the electrons form electron bands due to the interaction between the discrete energy levels of many individual atoms. The bands can be regarded as distributions of very closely packed quantum states. Electrons are fermions and only one electron can occupy each quantum state of the system. The overall band structure is characterized by the **density of states** function $D(E)$, which tells how many electrons can be in an energy range $E \dots E + dE$. The quantum states of the bands are filled up to the **Fermi level** E_F . The electrical properties of the material are determined by the position of the Fermi level (Figure 4). In semiconductors or insulators, the highest band containing

electrons is referred to as the **valence band** and the next empty band above it the **conduction band**. In metals, this distinction is not clear and the electrons in the uppermost band are named either **valence** or **conduction** electrons in different sources. In semiconductors, the band gap is relatively small and the energy separation between the valence and conduction bands in semiconductors can be overcome by thermal, electrical, or chemical excitations.

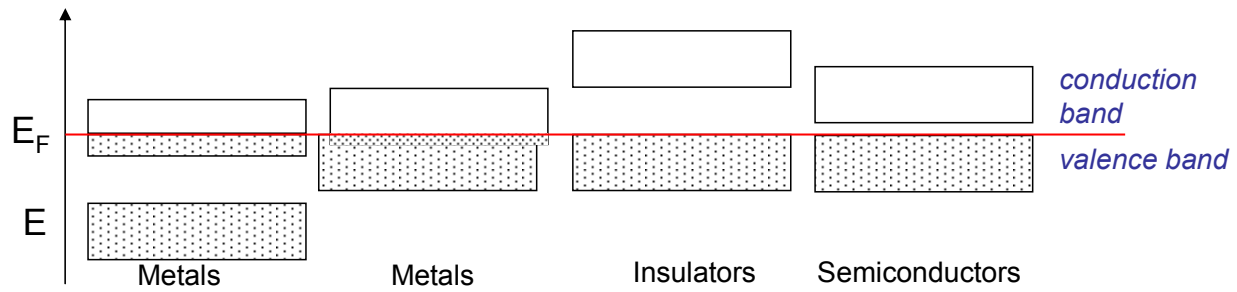


Figure 4. Classification of solids according to their band structure.

In detectors, the most relevant is the photoemission from metal surfaces or photoabsorption within semiconducting materials, as illustrated in Figure 5. The electron binding energy in metals is measured from the position Fermi level and one needs to take into account that additional energy – **work function** Φ – is required to completely remove the photoelectron from the material into vacuum, so that

$$E_{kin} = h\nu - E_b - \Phi. \quad (1-4)$$

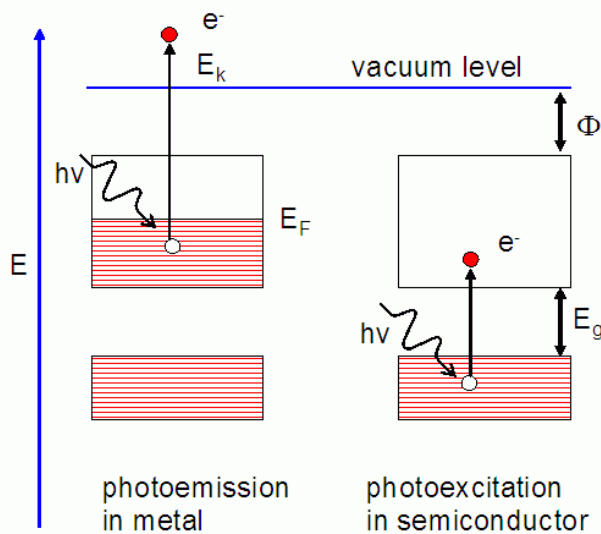


Figure 5. Two photoabsorption processes relevant to particle detection.

The work function corresponds to the minimum amount of energy needed to remove an electron from the metal and thus in photoemission from metals

$$h\nu_{\min} = \Phi . \quad (1-5)$$

Work functions of some materials are listed in Table 1. Note that the work function of a surface is strongly affected by the condition of the surface. The presence of minute amounts of contamination (less than a monolayer of atoms or molecules), or the occurrence of surface reactions (oxidation or similar) can change the work function substantially.

Table 1. Work functions of metals.

Metal	$\Phi(\text{eV})$
Aluminum	4.08
Beryllium	5
Cadmium	4.07
Calcium	2.9
Carbon	4.81
Cesium	2.1
Cobalt	5
Copper	4.7
Gold	5.1
Iron	4.5
Lead	4.14
Magnesium	3.68
Mercury	4.5
Nickel	5.01
Niobium	4.3
Potassium	2.3
Platinum	6.35
Selenium	5.11
Silver	4.73
Sodium	2.28
Uranium	3.6
Zinc	4.3

In semiconductor-based detectors, we are not interested in removing the charge carriers completely from the material, but in lifting a valence-band electron to the conduction band and creating electron-hole pairs. These electrons and holes can then drift through the material and be collected on electrodes. The minimum photon energy for creation such an electron-hole pair is

$$h\nu_{\min} = E_g , \quad (1-6)$$

where E_g is the band gap of the material.

2.1.2 Other processes

The **Compton effect** is essentially an elastic collision between a photon and an electron; during this interaction, the photon gives a fraction of its energy to the electrons. The cross section for this effect decreases with increasing energy, but the decrease is less rapid than for the photoelectric effect.

In the ***pair-production*** effect, a high-energy photon near a nucleus gives up its energy to produce an electron-positron pair. The photon energy goes into the rest-mass energy and the kinetic energy of the electron-positron pair. The minimum energy necessary for this effect is set by elementary relativistic considerations at the value of 1.022 MeV, an amount equivalent to two electron rest masses. The positrons can encounter electrons in the surrounding atoms and annihilate, producing again radiation. The electrons of the pair, however, can be collected and measured as electric currents.

Although all three processes can compete with each other, the photoelectric effect dominates at low photon energies below 1 MeV (Figure 6).

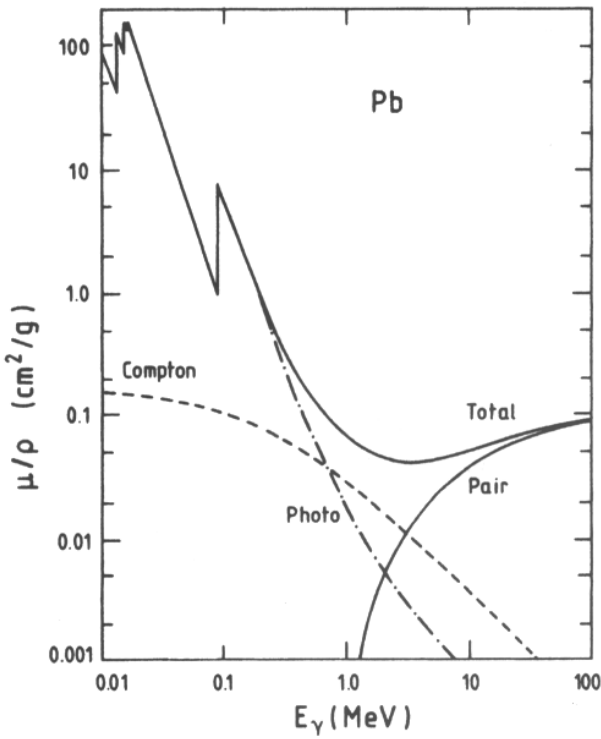


Figure 6. Mass absorption coefficient for various processes in lead.

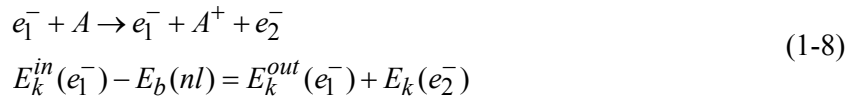
2.2 Electrons and ions

While photons can lose all their energy in interaction (absorb), massive particles like electrons lose only a fraction of it (Figure 7). The following are the main processes:

- 1) **Excitation by inelastic collisions:** a bound electron is promoted from its atomic orbital nl to a less tightly bound orbital $n'l'$, and the incident electron loses energy approximately by



2) **Ionization by inelastic collisions:** a bound electron is ejected from the atom, as in photoelectric effect.



Here only the sum of the energy loss of the incident electron and the kinetic energy of the second electron is uniquely determined; both individually can take a range of values.

3) **Elastic collisions:** electron interacts with the atom or its nucleus as a whole, not with a particular bound electron. The energy and momentum are redistributed, but no ionization or excitation occurs. This process is not useful for particle detection.

4) **Bremsstrahlung:** electron emits radiation as it accelerates/decelerated within the atom or solid, according to the Maxwell equations.

5) **Cerenkov radiation:** electromagnetic radiation emitted when a charged particle passes through an insulator at a speed greater than the speed of light in that medium. The characteristic "blue glow" of nuclear reactors is due to Čerenkov radiation. The effect is used in s.c. Cerenkov counters to detect very high energy particles.

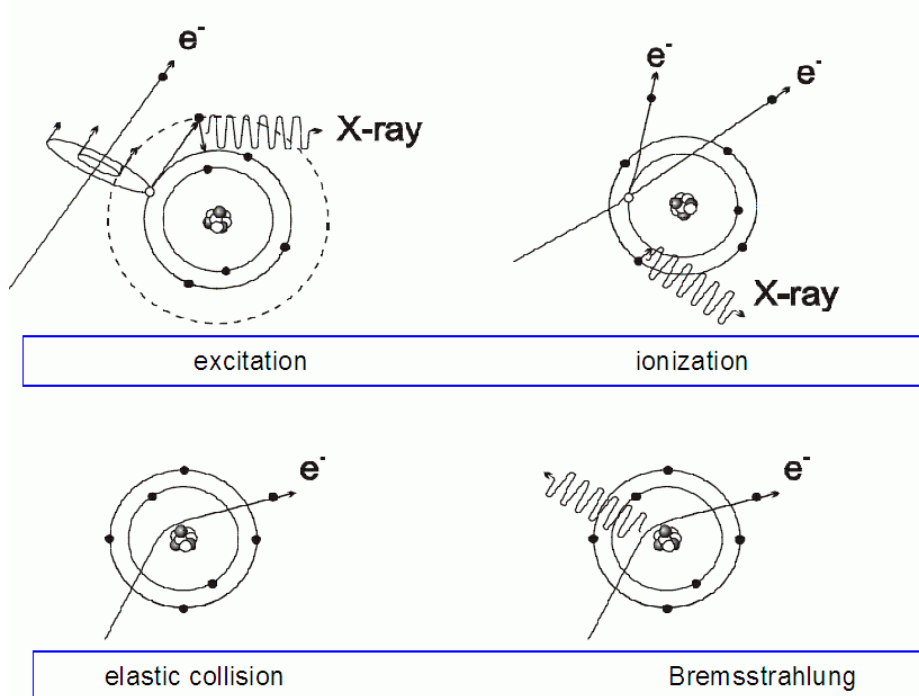


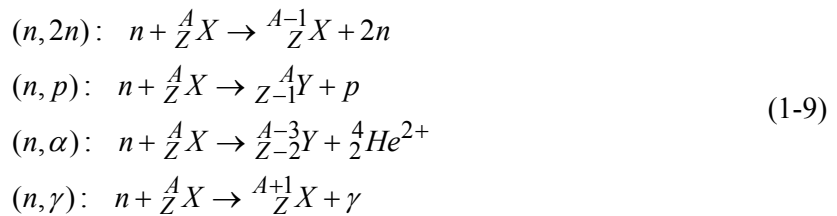
Figure 7. Interaction of electrons with matter [M. Miglierini].

For heavy charged particles as ions, inelastic excitation and ionization by heavy charges particles are also most important processes in detectors. Elastic scattering of ions can take place as a *Rutherford scattering* between the two types of nuclei, redistributing energy and momenta, but not creating free charged particles.

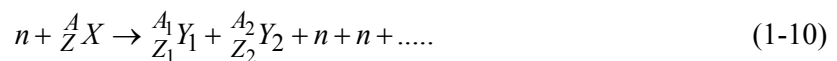
2.3 Neutrons

As neutrons do not carry electric charge, they interact only with atomic nuclei via nuclear forces in the following processes (Figure 8):

- 1) Inelastic scattering:** The nucleus is excited which is followed by the emission of a γ -quantum of radiation.
- 2) Elastic scattering:** No internal excitation of the nucleus occur, takes place mostly between fast neutrons and low atomic number elements (“billiard ball effect”).
- 3) (Radiative) capture:** the incident neutron is absorbed into the nucleus, which leads to several possible reactions:



- 4) Fission:** Dissipation of energy in the fission reaction can cause ionization of the medium.



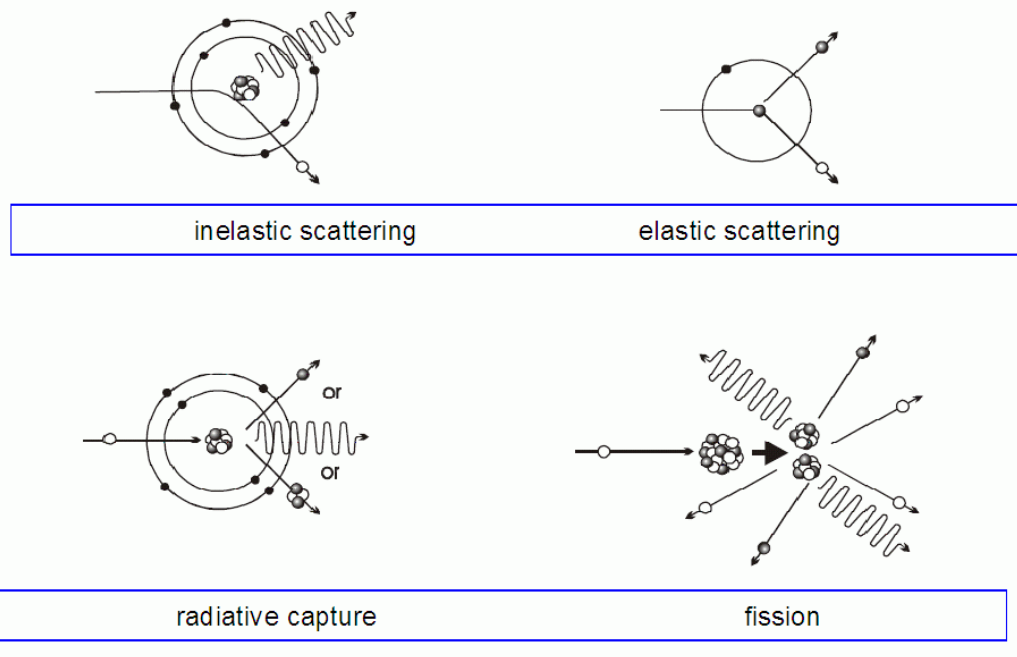
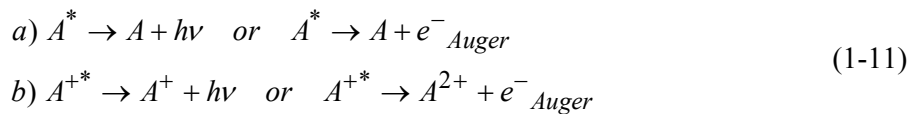


Figure 8. Interaction of neutrons with matter [M. Miglierini].

2.4 Relaxation processes

The processes described above often leave the atom or ion in an *excited state*. For example, high-energy radiation has a high probability to remove an electron from an inner shell of the atom, either to continuum or to an empty bound orbital. The resulting state is unstable, and will decay into a state of lower energy. Below are the relaxation processes for excited atoms (a) and ionized atoms (b). Figure 7 showed the relaxation in the form of *x-ray emission*, but it can also take place as *Auger electron emission*:



In larger quantum mechanical systems such as crystals or organic molecules, the variety of energy dissipation processes is larger, for example by molecular vibrations or phonons. Figure 9 illustrates the decay of such a quantum-mechanical system after inner-shell photoionization. Atomic X-ray emission produces characteristic x-rays. Other forms of radioactive decay are *fluorescence* (fast) and *phosphorescence* (slow), that involve relaxation of the excited state by other means, so that the energy of the emitted photon can be much smaller than of the primary photon or other ionizing particle. Such phenomena are used in for example *scintillation counters* to shift the wavelength into

a range that can be more effectively converted into free electric charge. Auger processes release additional electrons from the system, thus increasing the free charge. Auger processes can occur in cascades, where the system decays step-by-step to lower energy states, in each step the inner-shell holes move towards outer shell and additional electrons are emitted.

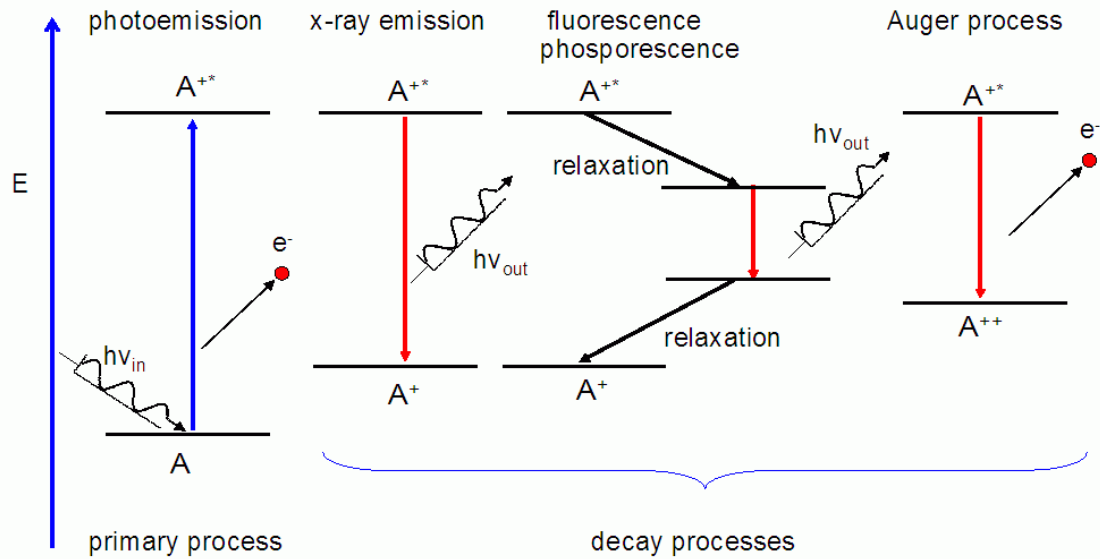


Figure 9. Secondary processes after photoionization.

3 Units and detector characteristics

3.1 Useful units

The energy of radiation above the visible range is usually measured in electron volts (eV), which is the kinetic energy of an electron when it is accelerated in a potential difference of 1V.

$$1\text{ eV} = 1.602 \times 10^{-19} \text{ J} \quad (2-1)$$

In high-energy particle detection, this energy unit is sometimes also used to derive the units for the rest mass of a particle (using $E=mc^2$):

$$1\frac{\text{eV}}{c^2} = 1.78 \times 10^{-36} \text{ kg} \quad (2-2)$$

and for momentum p . Since the total relativistic energy is

$$E^2 = p^2 c^2 + m^2 c^4, \quad (2-3)$$

one can measure momentum in the units of eV/c:

$$1\frac{\text{eV}}{c} = 0.535 \times 10^{-27} \frac{\text{kg} \cdot \text{m}}{\text{s}}. \quad (2-4)$$

A large fraction of particle detectors are used to study radioactive sources, which are characterized by their **activity** in the SI units of becquerel:

$$1\text{ Bq} = 1\frac{\text{decay}}{\text{s}} \quad (2-5)$$

or *curie*:

$$1\text{ Ci} = 3.7 \times 10^{10} \frac{\text{decays}}{\text{s}} \quad (2-6)$$

Calculating the activity of a radioactive sample can be done using the *decay constant* λ

$$\frac{dN}{dt} = -\lambda N \quad (2-7)$$

where N is the number of radioactive nuclei. The inverse of λ is the *mean lifetime* of the isotope:

$$\tau = \frac{1}{\lambda}, \quad (2-8)$$

but it is customary to use instead the *half-life* which is the time it takes for half of the nuclei to decay:

$$t_{1/2} = \tau \ln 2 = 0.693\tau . \quad (2-9)$$

Quantities that can be easily measured are also the *energy dose (absorbed dose)*, In SI units one *gray* is the absorption of one joule of radiation energy by one kilogram of matter:

$$1 \text{ gray} = 1 \frac{\text{J}}{\text{kg}} \quad (2-10)$$

The *exposure (ion dose)* measures the charge liberated in the sample by ionizing radiation.

Still commonly used unit is *röntgen*: the amount of radiation required to liberate positive and negative charges of one electrostatic (CGS) unit of charge in 1 cm³ of air at standard temperature and pressure (STP). This corresponds to the generation of approximately 2.08×10^9 ion pairs and is in proper units:

$$1 R = 2.58 \times 10^{-4} \frac{\text{C}}{\text{kg}} \quad (2-11)$$

3.2 Common detector characteristics

3.2.1 Temporal properties

In counting the number of particles, in practice one measures the *flux* of particles, defined as

$$I = \frac{n}{tA} \quad (2-12)$$

where n is the number of particles penetrating area A (the effective active area of the detector) in a time interval t .

In general, a single particle is detected in a measuring instrument by the charge Q liberated during the passage of the particle or photoabsorption by one of the processes described in Section 2. This charge is guided towards collecting electrodes by means of electric and/or magnetic fields. The collection time t_c of the released charge can vary from a few nanoseconds (photomultiplier tubes) to milliseconds in gas ionization chambers.

We take the moment of the arrival of particle as $t=0$ and regard the detector as an electronic circuit. The instrument will produce a current between times $t=0$ to t_c , so that

$$Q = \int_0^{t_c} I(t) dt .$$

If the timing information about the arrival of the particle is unimportant, then the simplest way of recording the detector output is a measurement of the average dc current delivered by the detector. This serves as a measurement of the incident flux, when the charge liberated by each particle is the same. On the other hand, if the free charge created by a particle is proportional to its energy, then the detector measures the energy dose. This, s.c. **current mode**, is used *e.g.* in radiation dosimetry.

In many applications, however, the properties of single particles or their exact number is important, and to detect it one needs a variation in the detector output current after the arrival of each particle. In this, s.c. **pulse mode**, we can model the detector itself and the recording system as a simple ac-circuit (Figure 10):

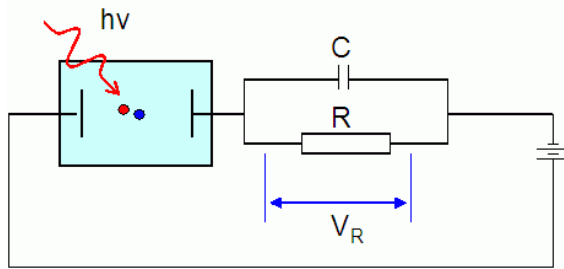


Figure 10. Simple ac-circuit model for a detector.

Before the photon arrives, there is no current through the circuit and $V_R=0$. The arrival of photon or a particle releases charge carriers that drift to the electrodes during $t=0 \dots t_c$. If the time constant of the circuit,

$$\tau = RC \quad (2-13)$$

is much shorter than the collection time ($\tau \ll t_c$), then the voltage $V_R(t)$ follows closely the arrival of the charge carriers to the electrodes and falls to zero by the time t_c when all charge Q is collected. On the other hand, if $\tau \gg t_c$, then the voltage V_R keeps rising until $t=t_c$, when it reaches its maximum value

$$V_{\max} = \frac{Q}{C} \quad (2-14)$$

The capacitor then discharges through the resistor R and the voltage falls to zero. Thus, in this regime of $\tau \gg t_c$, a voltage pulse is created with V_{\max} proportional to the charge, which is suitable for measuring the particle energy.

When simply counting particles, the ***maximum frequency*** of the detector is more important than determining the exact amounts of charge Q. In this case we are likely to use RC-circuits with $\tau \ll t_c$ and then the maximum frequency is limited by the time t_c it takes the charge carriers to leave the active area. The time of this cycle is determined by the ***drift velocity v*** of the carriers over the dimension D of the active media:

$$t_c = \frac{D}{v} \quad (2-15)$$

and thus the maximum counting frequency

$$f_{\max} \approx \frac{v}{D} \quad (2-16)$$

Other factors, thus as delays in electronic circuits and ADC conversion times can lower the maximum frequency considerably. A measure that accounts for all these effects is the ***dead time***, which is the time period after the arrival of a particle, during which the detector is unable to process another particle.

3.2.2 Statistical properties

The distribution of pulse heights $N(V_{\max})$, measured over a certain period of time, is called a ***pulse height spectrum***. If one wants to determine the particle energy E from the pulse height spectrum, one needs to know the average (e^- & e^+ charge) ***pair production energy δ*** in the detector material so that

$$Q = \frac{E}{\delta} e \quad (2-17)$$

Such ***particle energy spectrum N(E)*** is shown in Figure 11. The distribution Figure 11 illustrates another important detector characteristic, its ***resolution***. The photons that were detected originated from the O K_α x-ray emission line that all have the energy very close to 525 eV. Ideally, these would always produce equal amounts of charge Q. In reality, the pulse amplitudes fluctuate and the measured distribution $N(E)$ is broad, its ***full-width-at-half-maximum (FWHM) Γ*** is about 100 eV.

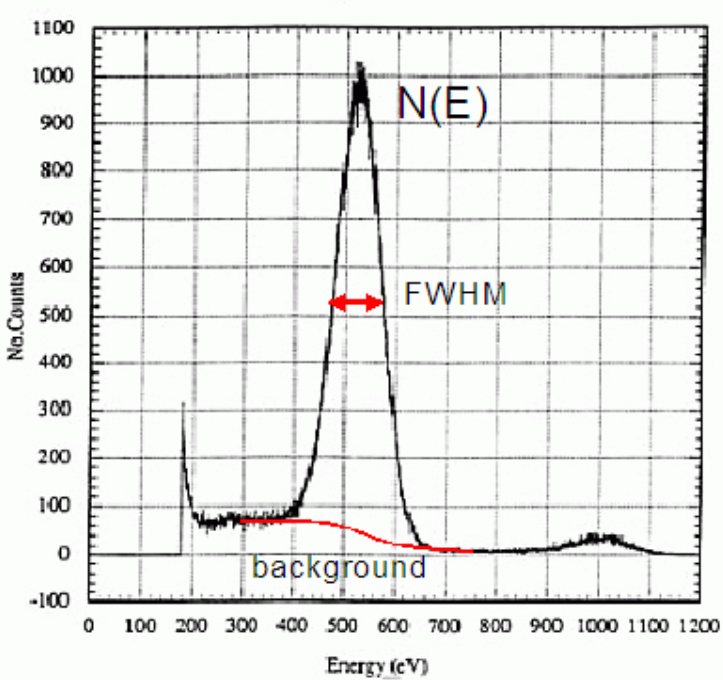


Figure 11. Pulse Height Distribution of Oxygen K_α line, measured with Ortec IGLET-X™ Germanium (HPGe) detector [Ortec website].

The **resolution** is usually defined as a unitless quantity:

$$R = \frac{\Gamma_{FWHM}}{\bar{E}} \quad (2-18)$$

The resolution limits the accuracy of our energy measurement – the larger R, the less accurate result. Its origin can be explained by regarding the pair production statistically. The charge Q is generated by a chain of processes described in Section 2, for example photoionization followed by electrons losing gradually energy in collisions with atoms, each time creating more free carriers.

If all of the energy lost by ionizing radiation or particles in a detector were spent for pair creation, the number of free charge pairs created by one absorbed x-ray photon of energy $h\nu$ would always be exactly:

$$n = h\nu / \delta \quad (2-19)$$

and no statistical fluctuations would occur. However, part of the photon energy is also spent for non-ionizing excitations (thermal motion, molecular vibrations, photons in crystals,...), thus reducing the number of electron-hole pairs n . If the thermal excitations are completely unrelated to the ionizing pair creation then the statistical distribution of the number of pairs would follow the

Poisson statistics, according to which the *variance* in the number charge pairs n would be equal to its mean value:

$$\sigma^2 = \bar{n} \quad (2-20)$$

In fact, the individual events creating pairs or thermal excitations are often correlated in some extent and also the electrons in atoms have discrete binding energies. Therefore, the Poisson statistics (that assumes completely independent events) gives wrong predictions. A (usually empirical) **Fano factor** F is introduced to modify the Poisson relation. The corrected equation for the variance can be written as

$$\sigma^2 = F \bar{n} \quad (2-21)$$

- $F=0$: no fluctuations in the number of charged pairs/particle
- $F=1$: Poisson statistics applies fully

The actual values of Fano factors vary from about 0.06 in semiconductor materials to 1 in scintillation counters. For large \bar{n} (>20) the Poisson distribution function resembles that of the normal (Gaussian) distribution with maximum at \bar{n} and with the width given by the standard deviation:

$$\begin{aligned} \sigma &= \sqrt{F\bar{n}} \\ \Gamma_{FWHM} &= 2\sqrt{\ln 2} \sigma = 1.665\sigma \end{aligned} \quad (2-22)$$

Thus the resolution

$$R = \frac{\Gamma_{FWHM}}{\bar{n}} = 1.665 \frac{\sqrt{F\bar{n}}}{\bar{n}} = 1.665 \sqrt{\frac{F}{\bar{n}}} \quad (2-23)$$

As R is an unitless quantity, its value does not change if we convert the distribution function to the energy scale: assuming that the detector is linear and the pair-creation energy is δ , the peak maximum energy

$$E_{\max} = \delta \bar{n} \quad (2-24)$$

and Γ_{FWHM} in the energy scale as

$$\Gamma_{FWHM} = 1.665\sigma = 1.665\delta\sqrt{F\bar{n}}, \quad (2-25)$$

we still have for the resolution

$$R = \frac{\Gamma_{FWHM}}{E_{\max}} = \frac{1.665\delta\sqrt{F\bar{n}}}{\delta\bar{n}} = 1.665 \sqrt{\frac{F}{\bar{n}}} \quad (2-26)$$

and in our example of photoionization,

$$R = 1.665 \sqrt{\frac{F\delta}{h\nu}} \quad (2-27)$$

Small Fano factors and pair production energies improve the energy resolution. Other factors, such as electronic noise, broaden the distribution and worsen the resolution.

3.2.3 Other properties

If the incident particle energy E_0 increases, also the mean value \bar{E} of the measured distribution increases. In general for any measured quantity X , $\bar{X} = f(X_0)$. If this relationship is of the type

$$\bar{X} = cX_0, \quad (2-28)$$

then the detector is **linear** in respect of that quantity. There is usually a region of linearity, outside which the response is distorted due to changes in efficiency, saturation etc.

Assume a radioactive element emits a single γ -quantum in isotropic direction. We are interested in the probability of detecting that particle; or in **detection efficiency ε** . It consists of two factors:

1) **Transmission**, the solid angle from which the particles can be collected:

$$T = \frac{\Omega}{4\pi} \quad (2-29)$$

For example, a perpendicular detector surface with area A , at a distance R away from the point source, gives

$$\Omega = \frac{A}{R^2}, \quad \text{if } A \ll R^2. \quad (2-30)$$

2) The **intrinsic efficiency** of the detector ε_i . $\varepsilon_i < 1$, if not every particle impinging on the area A creates a measureable pulse. The total detection efficiency,

$$\varepsilon = T\varepsilon_i. \quad (2-31)$$

The creation of a "measureable pulse" means that sufficient charge Q must be released by a single incoming particle. This can again be described by two important detector properties:

- **Quantum efficiency QE**, which is the probability that the primary ionization process takes place after a particle enters the detector, for example that a photon absorbs and emits a photoelectron from a metal surface or that the first electron-ion pair is created in gas. In photon detectors, QE is a function of photon energy as seen from Figure 12:

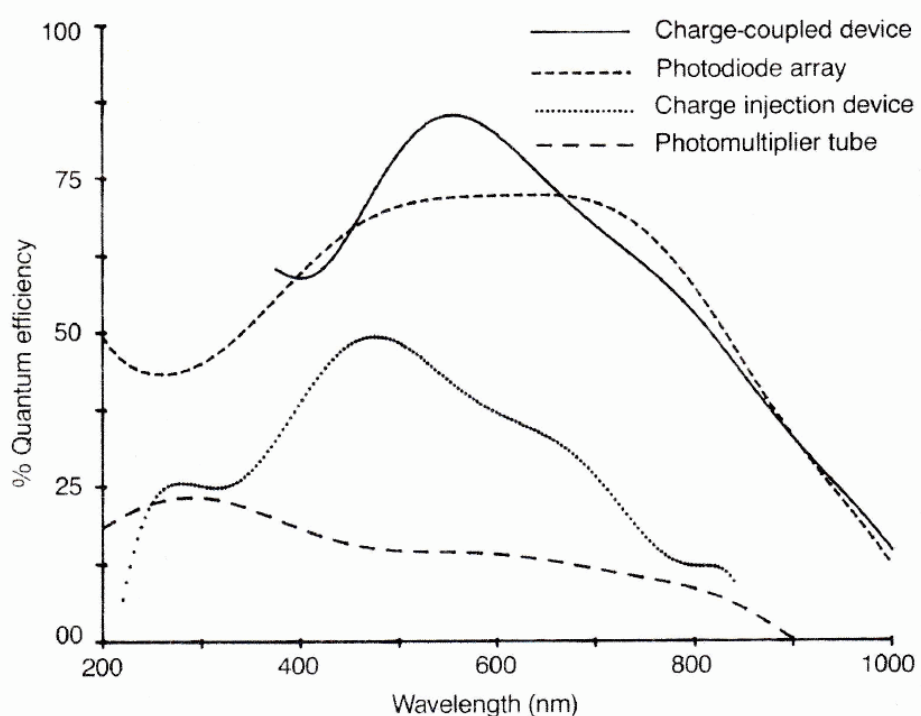


Fig. 6, Sweedler et al., Anal. Chem. (1988) 60, 282A

Figure 12. Quantum efficiencies of light detectors.

- **Gain G.** In general, gain is a measure of the ability of an electronic circuit to increase the amplitude or power of a signal. In this sense, most detectors are amplifiers, the amplification process being the creation of a cascade of secondary charge pairs after the primary ionization has occurred (Figure 13). Gain is the final number of charge pairs per one primary pair. The amount of charge released per one particle is then, *in average*:

$$\bar{Q} = (QE \times G)e \quad (2-32)$$

The values of gain can be very large, in photomultipliers for example $G > 10^6$ and in Geiger-Müller counters around 10^{11} .

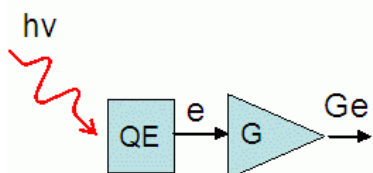


Figure 13. Quantum efficiency and gain.

4 Gas-filled detectors

4.1 Electrons and ions in gases

4.1.1 Motion of free charges

The motion of both electrons and ions in gases is a combination of two processes – *diffusion* – random thermal motion through collisions with other particles, and *drift* – directional motion along the lines of electric field, if present. In gas-filled detectors, the drift velocity determines, how fast the charge is collected; and the rate of diffusion determines, how far the charge can spread out before collection. The latter quantity is important, if we need to determine also the point where the ionization occurred.

If a cloud of ions in a gas is put in an electric field of strength E , it starts to move with an average drift velocity v_D^+ along the electric field lines. The drift velocity of ions depends linearly on the field strength E and on the gas pressure p . The **mobility** of the ions is defined so that

$$v_D^+ = \mu^+ E \frac{p_0}{p} \quad (4-1)$$

where p_0 is the normal pressure.

The drift velocity v_D^- of electrons as a function of field strength is much more complicated (Figure 14). In general, it reaches saturation at rather low field strengths, i.e. v_D^- stops increasing with E or even starts to decrease. The point of saturation depends strongly on even small admixtures of other gases in the main gas. For example, adding 1% of N₂ to Ar gas increases v_D^- from 0.5 to 2.3 cm/μs at E=1kV/cm. Since the operation of the detector is more stable if the electron drift velocity has reached the saturation value, at a certain field strength one can use admixtures of gases in order to “tune” the saturation velocity.

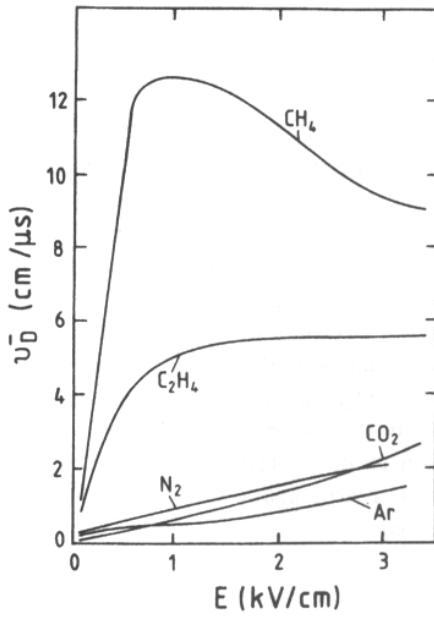


Figure 14. Diffusion velocity of electrons in gases.

The diffusion process in its fundamental form is described by Fick's first or second law, depending on whether the concentration of the diffusing particles is constant over the whole volume or not. In our case, the ions and free electrons are created by particles and recombine at electrodes, so Fick's second law should be used:

$$\frac{\partial \phi}{\partial t} = D \times \nabla^2 \phi \quad (4-2)$$

where ϕ is the concentration of ions and D is the **diffusion coefficient** [in m²/s]. As a more concrete example, let's assume all ions are created at a single point with coordinates (0,0,0) at the time t=0. Initially, the density distribution function $N(x,y,z)$ of ions is thus a delta-function, which starts to spread out due to diffusion. It assumes a Gaussian form that has a standard deviation along one coordinate as

$$\sigma_x = \sqrt{2Dt} \quad (4-3)$$

The ion diffusion coefficient increases with the average thermal velocity u :

$$u = \sqrt{\frac{3k_B T}{m}}, \quad (4-4)$$

where k_B is the Boltzmann constant, T temperature and m the mass of ions. Therefore the ions “spread out” faster if their mass is smaller or the gas temperature is higher. During diffusion, ions

constantly collide with the gas molecules, with a *mean free path* λ between the collisions depending on the gas concentration N and the collision cross-section σ .

$$\lambda = \frac{1}{N\sigma(\varepsilon)}. \quad (4-5)$$

For some common gases, ion kinematic properties are listed in Table 2.

Table 2. Thermal velocity, diffusion coefficient, mobility and mean free path of ions in their own gases at normal conditions.

Gas	Mass number	u (cm/s)	D^+ (cm ² /s)	μ^+ (cm ² /V s)	λ (10 ⁻⁵ cm)
H ₂	2.02	1.8×10^5	0.34	13.0	1.8
He	4.00	1.3×10^5	0.26	10.2	2.8
Ar	39.95	0.41×10^5	0.04	1.7	1.0
O ₂	32.00	0.46×10^5	0.06	2.2	1.0
H ₂ O	18.02	0.61×10^5	0.02	0.7	1.0

The mean free path of electrons is larger than for ions, due to their higher velocity and small particle size. Therefore they also gain much more energy between collisions in electric field than ions. In particular, for electrons with a certain kinetic energy in the order of 1 eV, their Broglie wavelength is about twice the diameter of the atoms (the extent of the valence orbital). Under such conditions, the atom becomes nearly transparent to the electrons and the collision cross-section goes through a *Ramsauer minimum*; in other words, the mean-free path of electrons is strongly energy-dependent and becomes very large at the Ramsauer minimum.

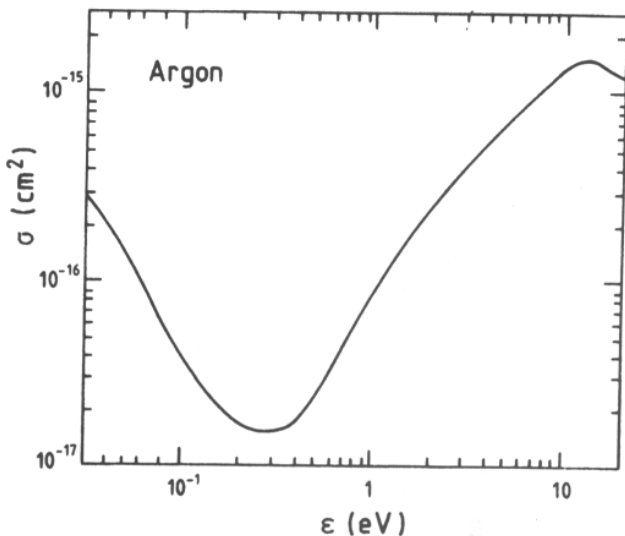


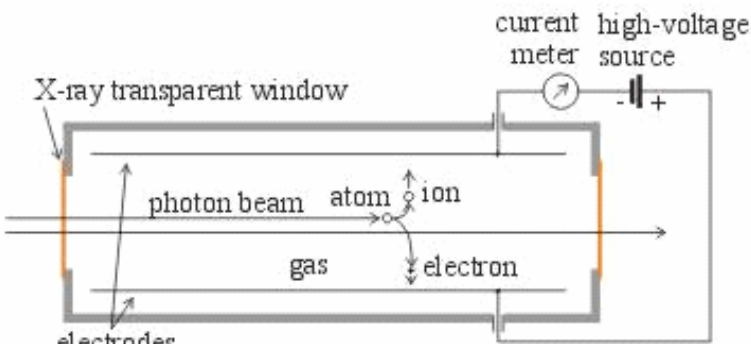
Figure 15. Electron-atom collision cross-section in argon as a function of electron energy.

4.1.2 Recombination and capture

The ions and electrons produced during the ionization process can be neutralized before being collected on the electrodes. Positive ions can recombine with electrons and negative ions. In addition, some gas molecules such as O₂ and CH₄ can capture free electrons of low energy (≈ 1 eV). This process is also detrimental for the detector's performance and therefore, specially for large-volume detectors, special care must be taken to purify the gas from e.g. O₂ contamination.

4.2 Operational regions

The principal components of a gas-filled detector are shown in Figure 16.



© AG FRAHM, BUGH WUPPERTAL / MR

Figure 16. Principal layout of an ionization chamber.

Typically such a detector consists of two electrodes with a gas filling the space between them. Ionizing particles pass the gas and release electron-ion pairs that start drifting towards the electrodes. The device can be operated in a pulse or current mode, in the first case the pulses of individual particles are measured (*pulse chamber*), in second, the average dc current is recorded (*current chamber*).

In Section 2 we considered the processes creating the electron-ion pairs. In general, through a chain of processes, the energy of the primary particle was spent creating electron-ion pairs, eventually a large number of them with low kinetic energy, that then start drifting towards the electrodes. Now we should also consider the effect of the applied electric field. The electrons have a much larger mean-free path than ions and, if put in a strong field, can achieve kinetic energy $E_k > I(A)$ so that they are again able to ionize gas atoms. Newly released electrons are again accelerated in the field etc. If this happens, an ***electron avalanche*** (aka Townsend avalanche) towards the anode takes place and as a result, a very large number of electron-ion pairs is eventually created just by a single ionizing particle. This process is also called ***gas amplification***.

The electron avalanche is also referred to as the secondary process, not to be confused by the relaxation and secondary processes treated in Section 2.4. In these processes, ionization is still a result of the energy dissipation of the initial event, whereas in an avalanche, the energy for ionization is taken from the electric field.

At even higher field strengths, also the atoms can become excited in electron-atom collisions so that they emit photons. Photons can travel larger distances before reabsorption and thus in turn create new ionization centers elsewhere, quickly spreading the avalanches over the whole volume (Figure 17)

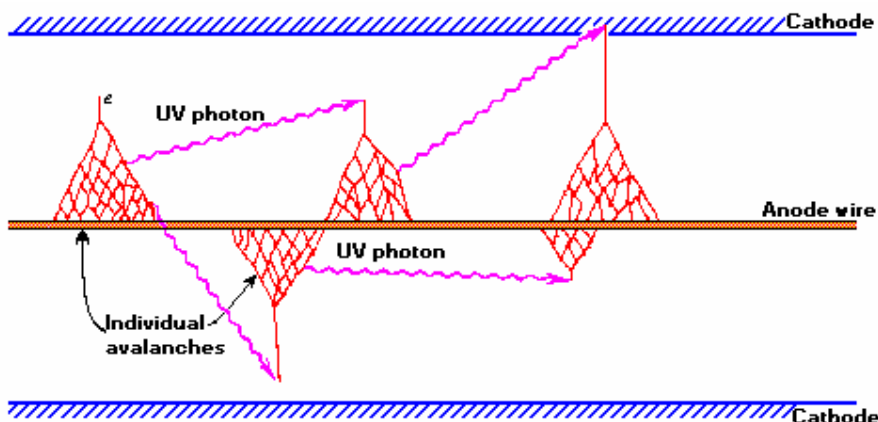


Figure 17. Avalanches at high electric field strengths.

Thus, the behaviour of a gas-filled detector depends crucially on the field strength, which largely determines its operational mode. Figure 18 shows an example of a gas-filled chamber, number of pairs vs. voltage.

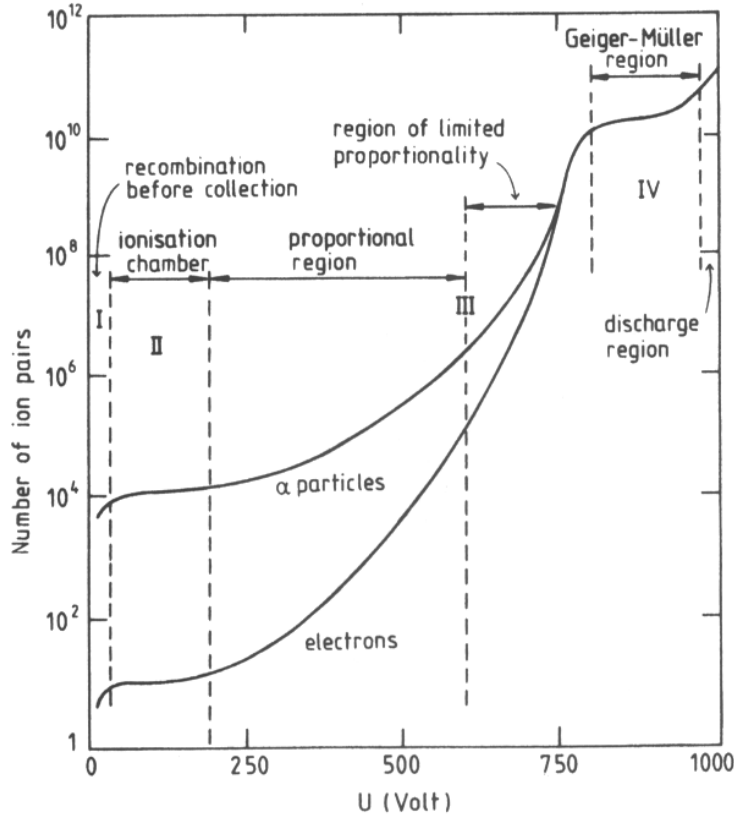


Figure 18. Operating regions of a gas-filled detector

On the curve, one can see different regions:

I. Recombination region:

- The drift velocity of charges is so small that they recombine before reaching the electrodes.
- No detector operates in this regime.

II. Ionization region:

- electric field is sufficient to ensure that all charges are collected.
- no gas amplification (no avalanches) takes place, gain $G=1$.
- **ionization chambers** operate in this region.
- detector output signal's amplitude is proportional to particle's energy (energy range >10 keV).

- weak signal – only strongly ionizing particles are detected.
- can work in pulse counting or in current mode, usually used to measure large particle fluxes.
- can detect neutrons (BF_3 gas).

III. Proportional region:

- all charges are collected.
- gas amplification takes place, avalanche clusters appear.
- number of pairs produced ($G \approx 10^2 - 10^5$) is proportional to the particle's energy.
- **Proportional counters** operate in this region.
- suitable for any type of ionizing particles.
- detection of low-energy ($< 10 \text{ keV}$) particles is possible due to large amplification.
- preserve the information about the position of the initial ionization (multiwire chambers).
- special care to ensure proportionality (quenching gases such as methane).

IIIb. Region of limited proportionality:

- no counters operate in this region.

IV. Geiger Müller region:

- electron-ion pair production is independent on the type of the incident particle.
- electric field is so strong that the avalanches continue to spread until further amplification becomes impossible due to high density of positive ions around the anode.
- gas amplification reaches saturation, $G > 10^7$ and proportionality no longer exists. The output signal does not depend on the incident particle's energy.
- **Geiger-Müller counters** operate in this region.
- operation point: $G > 10^7$
- signal completely independent of primary ionisation.
- no local avalanches exist any longer.
- chain reaction (Figure 17):

atoms become excited in collisions and emit photons.

photons absorb and emit new photoelectrons.

secondary electrons are accelerated in the very high field regions.

- The chain reaction “dies” since the discharge effectively lowers the electric field after enough particles are ionized.
- to help stopping the discharge add quenching gas (typ. ~10%) with high photon absorption cross section (usually molecular vapors like alcohol).
- detection of any type of ionizing particle is possible.
- high sensitivity, simple design – portable.
- information only about the number of particles.
- large dead-time = low counting rates.
- degradation of gas quality = limited lifetime.
- avalanches spread everywhere = no spatial information can be obtained.



Figure 19. A portable Geiger-Mueller counter.

4.3 Avalanche ionization

As seen above, the formation of electron-ion pairs in gas depends very strongly on the strength of electric field. Two typical electrode configurations are shown in Figure 20.

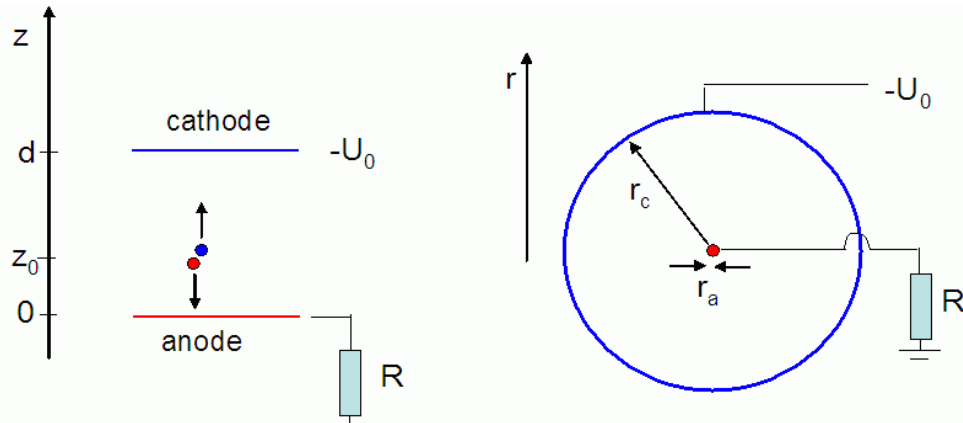


Figure 20. Gas-filled detector configurations.

In parallel-plate configuration, the field is constant across the volume,

$$E = \frac{U_0}{d}, \quad (4-6)$$

whereas in the cylindrical wire anode configuration, the field strength depends on r as

$$E(r) = \frac{U_0}{r \ln\left(\frac{r_c}{r_a}\right)}, \quad (4-7)$$

where r_a is the radius of the anode wire and r_c the radius of the cathode cylinder. $E(r)$ is largest near the central anode wire. Such a configuration, specially with very thin wire, allows to create strong fields near the anode with moderate voltages applied. In this case, the sequence of events is the following:

- a) An ionizing particle can form electron-ion pairs anywhere in the volume. The electrons then start drifting towards the anode. While they are far from anode, the field strength is not sufficient to give them enough kinetic energy between collisions to ionize gas atoms. Thus, an avalanche cannot form.
- b) When approaching the anode, field strength increases and at a certain distance, the drifting electrons will be able to ionize the atoms. The avalanche (gas multiplication process) begins.

- c) A cloud of free electrons and ions is formed. Electrons drift towards anode and ions away from it. The electrons continue to ionize more gas atoms.
- d) Due to diffusion, both electron and ion clouds spread out, eventually forming a drop-like shape encapsulating the wire. Electron cloud quickly shrinks around the anode.
- e) During a short time (ca 1 ns) electrons are collected on the anode. The ion cloud is repelled from the anode, expands and drifts towards the cathode wall.

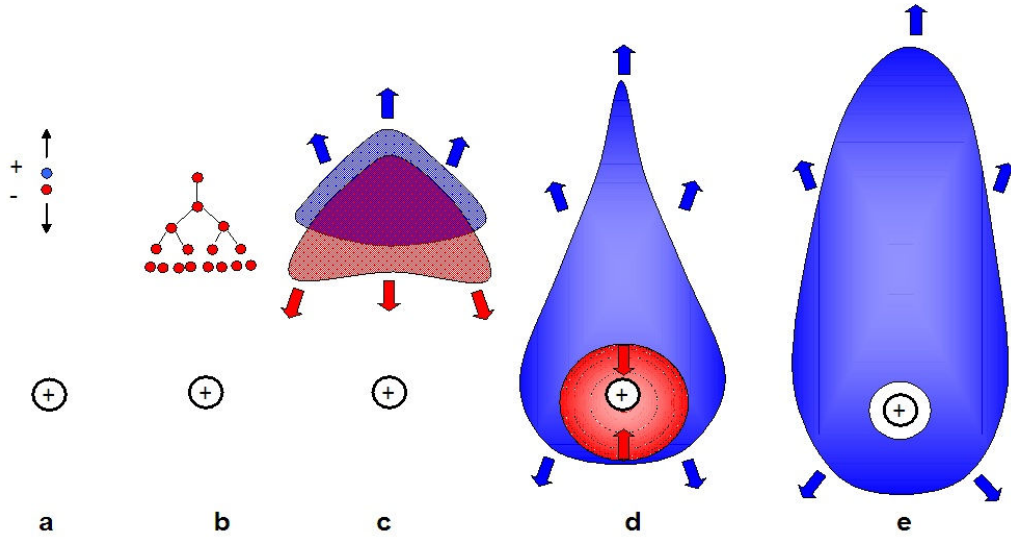


Figure 21. Electron avalanche formation near wire anode.

The motion of particles in an avalanche is a combination of drift and diffusion, is illustrated by computer modelling of avalanche formation in Figure 22. In the left, the trajectory of one single electron participating in an avalanche is plotted on a place perpendicular to the anode (red circle). Black dots show all positive ions created in this avalanche. The right panel shows the trajectories of all the electrons in the avalanche, plotted in the plane along the anode wire (red line).

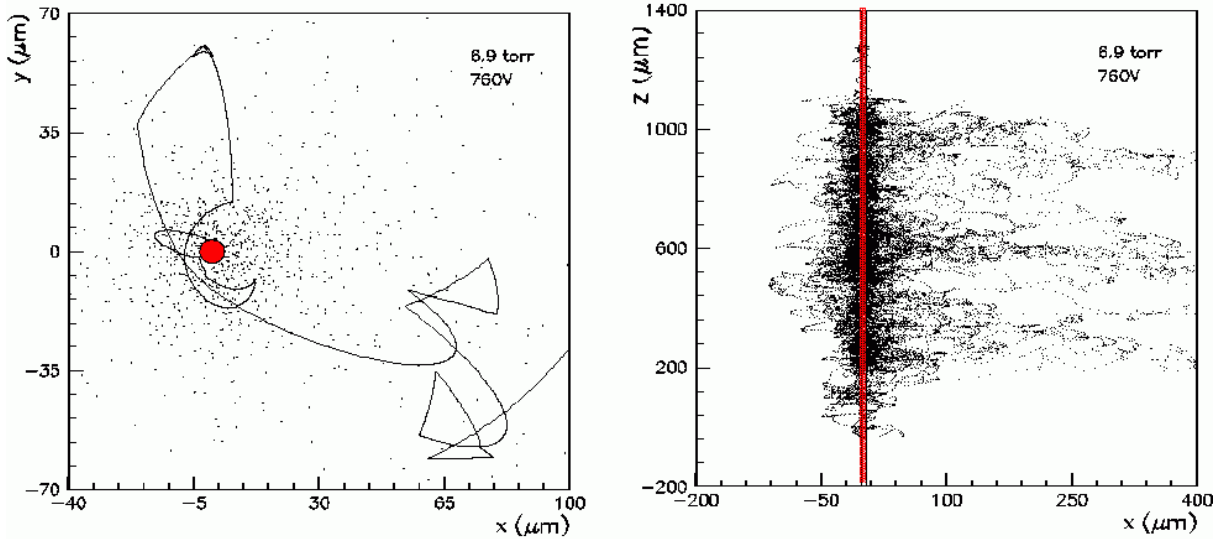


Figure 22. Modelling of electron avalanche near anode wire [H. Pruchova and B. Franek, <http://www.slac.stanford.edu/pubs/icfa/fall96/paper1/paper1.html>].

4.4 Pulse formation in an ionization chamber

Let us look at the pulse formation in an ionization chamber. The simplest form of such a chamber is a parallel plate capacitor filled with e.g. Argon (Figure 23):

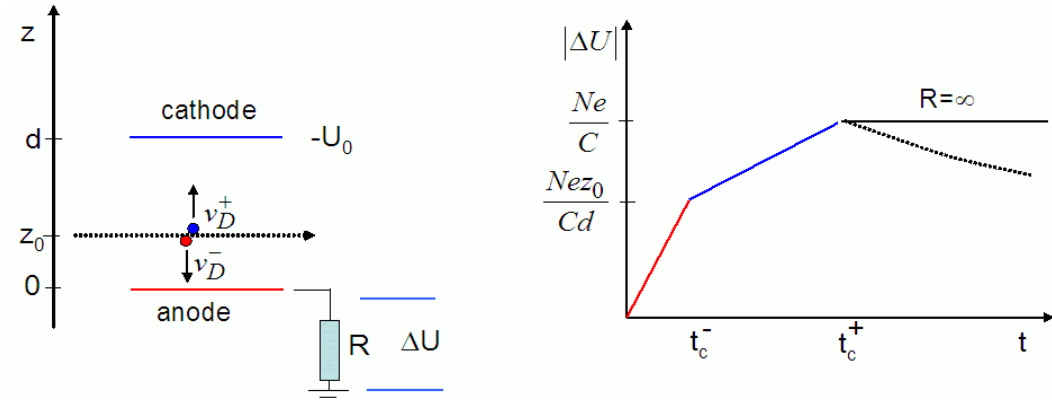


Figure 23. Left: parallel-plate capacitor as a detector, Right: Schematic pulse formation.

Let us choose the voltage U_0 so that all charge liberated along the path of the particle is collected, but the drifting electrons do not gain enough energy between collisions to further ionize the gas atoms. Then for an ionizing particle passing along the line $z=z_0$, we can calculate the amplitude of the voltage pulse on the resistor R . The potential energy stored in the capacitor is

$$E_C = \frac{1}{2} C U_0^2 \quad (4-8)$$

and as N charges q start drifting towards the plates, it will change as

$$\frac{1}{2}CU^2 = \frac{1}{2}CU_0^2 - N \int_{z0}^z qE_z dz, \quad E_z = \frac{U_0}{d} \quad (4-9)$$

From this, we obtain the change in the voltage after the charge has drifted by Δz along the z-axis:

$$\Delta U = -\frac{Nq}{Cd} \Delta z \quad (\text{if } \Delta U \ll U_0) \quad (4-10)$$

or, by using the drift velocity of ions and electrons, we obtain the time-development of the ion- and electron pulses as

$$\Delta U^+ = -\frac{Ne}{Cd} v_D^+ t, \quad \Delta U^- = -\frac{N(-e)}{Cd} (-v_D^-) t \quad (4-11)$$

(note that the ions and electrons drift in the opposite directions and have opposite charges, therefore the polarity of the pulses is the same). Thus, the capacitor senses the motion of the charge even before it is collected. Since the electrons drift much faster, first the electron pulse is collected within the electron collection time $t < t_C^-$ and then the voltage continues to rise more slowly until all the ions are collected during $t < t_C^+$. For example, in a parallel-plate chamber filled with Ar at normal pressure and $E=500$ V/cm, $t_c^- \approx 1 \mu s$, but $t_c^+ \approx 1 ms$.

As the second example, let's study the pulse formation in a wire chamber where most of the ions are created not by the ionizing particle itself, but in avalanches near the anode. In this case, regardless of where the initial event happened, most ions need to travel nearly the maximum distance from anode to cathode and the ion component ΔU^+ rises more slowly than in parallel plate configuration. On the other hand, most electrons need to be collected from a small distance (<0.1 mm) near anode and the electron component of the pulse rises very fast. The ratio of the electron and ion pulses does not depend on the point of initial ionization any more, since virtually all carries originate at anode:

$$\frac{\Delta U^+}{\Delta U^-} \approx \frac{\ln(r_c/r_a)}{\ln[(r_a + k\lambda)/r_a]} \approx \frac{\ln(r_c/r_a)}{k\lambda/r_a}, \quad (4-12)$$

where we assume that the average distance of electron creation is a small number k times the mean free path λ away from the anode wire surface. For example, if $r_a=0.1$ mm, $r_c=20$ mm and $k\lambda=0.02$ mm, the ion pulse is 25 times stronger.

4.5 X-ray imaging in a multiwire chamber

X-ray imaging is a standard method in medicine and non-destructive testing. The X-rays are normally detected using photographic film. In recent years new methods using digital detectors have been developed, one of these is a multiwire proportional chamber (MWPC) for detection of X-ray photons. This kind of detector was invented in the late sixties by Georges Charpak, Nobel laureate 1992, for tracking of charged particles in particle physics experiments. It has thereafter been refined and diversified in a large variety of devices exploiting various gas properties and improving on performances.

The MWPC allows to achieve high count rate, fully electronic detection and localization of ionizing radiation. Owing to their good efficiency, relative simplicity and localization accuracy, the use of gaseous detectors has spread in fields other than particle physics: medicine and biology and x-ray crystallography.

In its basic configuration, the MWPC consists of a set of thin, parallel anode wires stretched between the two cathode planes as shown in Figure 24. Application of a symmetric difference of potential between anodes and cathodes creates the electric field in the chamber (Figure 25). Electrons drift towards wires and avalanches take place near and around the individual wires. The electron part of the voltage pulses ΔU^- can be read out by separate electronic circuit from each wire, thus preserving the position information. Other methods of preserving the position information are the use of delay lines or resistive charge division; these are described in detail later (micromesh channel plate detectors).

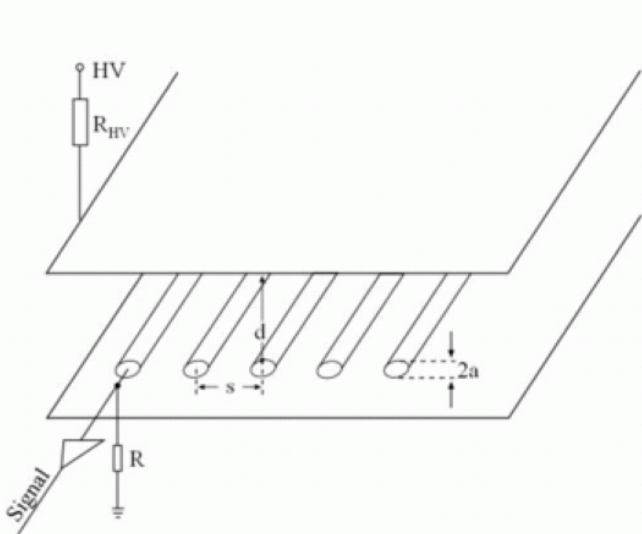


Figure 24. Principle of a 1D multiwire chamber.

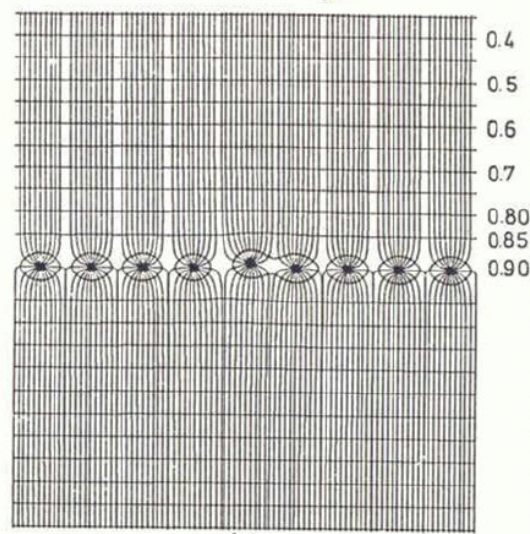


Figure 25. Electric field lines in an multiwire chamber.

The design in Figure 24 allows for the position information in one direction only, a more advanced design shown in Figure 26 can record the x-ray hit positions in two dimensions. In order to make faster and more accurate MWPC the gap between the anode wire and the cathode strips need to be made as small as possible. This allows the ions formed in the avalanche around the wire to quickly neutralise on the cathodes. The ministrip design shown below is built on top Cu strips etched on a PCB (printed circuit board).

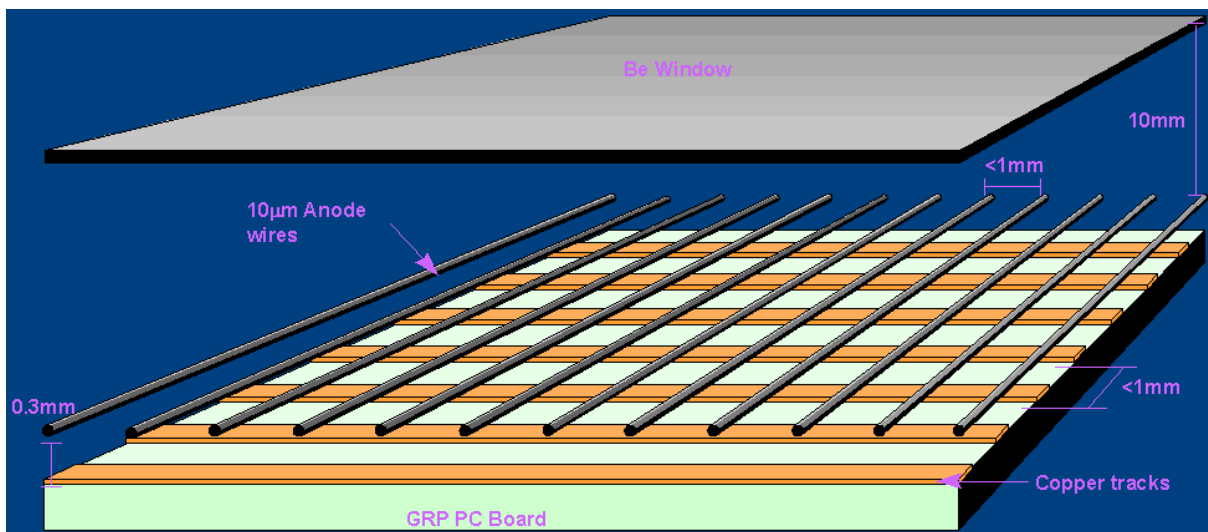


Figure 26. 2D multiwire (microgap) detector [Biological Detector Group at Daresbury Synchrotron, <http://www.srs.dl.ac.uk/OTHER/OW/BDET/microgap.html>].

4.6 Gas electron multiplier (GEM)

GAS ELECTRON MULTIPLIER GEM

Fabio SAULI CERN-EP-TA1-GD

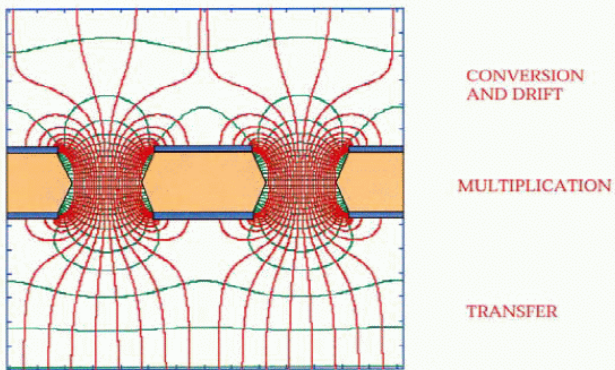


Figure 27. Gas electron multiplier [F.Sauli, NIM A386 531 1997]

A modification of a wire chamber is a device that is used for electron multiplication (Figure 27)[F.Sauli, NIM A386 531 1997]. Electrons travel from top to bottom in the electric field. The device has a special electrode on their path, an insulating kapton plate clad in Copper on both sides and with 70 μm holes through it. By applying a potential difference between the two copper sides an electric field as high as 100 kV/cm is produced in the holes acting as multiplication channels. The gas multiplication takes place while electrons move through the holes.

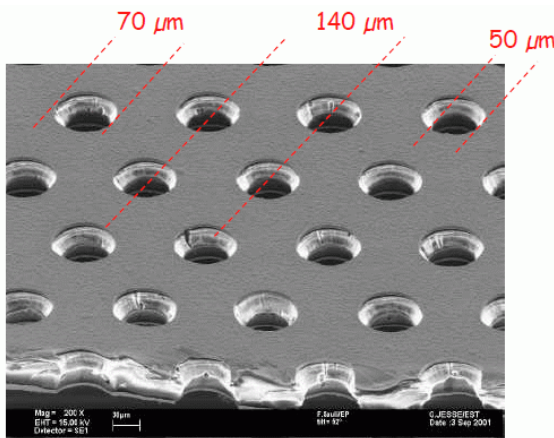


Figure 28. Scanning electron microscope image of the kapton "sieve" in GEM.

4.7 Detection of neutrons

Since neutrons do not directly ionize gas atoms, they are detected indirectly, after they have produced a charged particle or a photon that can then be detected by usual means. Several possible reactions can be used. For thermal neutrons, the most useful is the (n,α) reaction with ^{10}B :



^{10}B is a constituent of the BF_3 molecule, which can be used as a gas in the proportional counter or in an ionization chamber. The BF_3 detector detects the charged particles produced in reaction (4-13). Alternatively, the walls of the gas ionization chamber can be coated by boron, and the charged particles are released into the usual fill gas.

In fission chambers, the interior surface is coated by a fissile isotope. Neutrons interact with the wall material, producing charged products of a nuclear fission reaction. The production rate of these products is proportional to the number of neutrons detected.

5 Surface photoemission detectors

When photons are absorbed close to the surface of a solid material, photoelectrons can be ejected to the vacuum (see Figure 5), if the energy of the photon exceeds the work function of the material's surface:

$$hv > \Phi. \quad (4-14)$$

The common principle of operation of the detectors considered in this chapter is the creation of free charge in vacuum by photoelectric effect and multiplying and collecting it by means of electric fields.

5.1 Photocathodes and Phototubes

The simplest photoemissive device is a *phototube* – a device consists of a photocathode of large area, in the shape of a cylinder and with an anode wire on the axis, in a glass envelope (Figure 29). The anode wire collects the photoelectrons emitted from the cathode surface. Due to the very low gain of this device, it is normally operated in current mode, detecting high flux of light rather than single particle pulses.

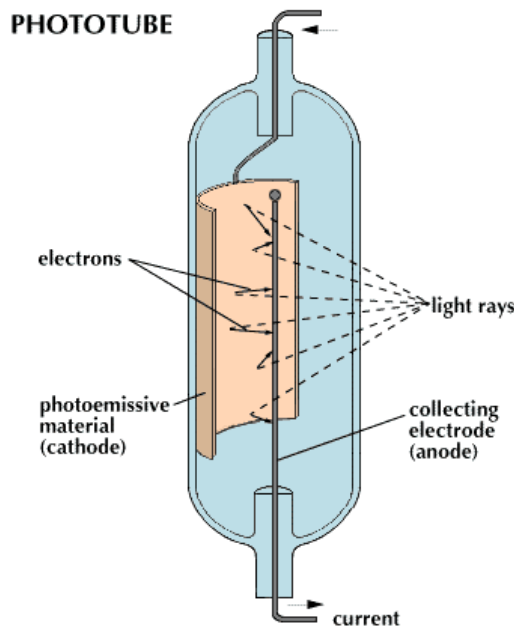


Figure 29. Principal layout of a phototube light detector.

In a *vacuum phototube*, the envelope under vacuum so that the electrons do not suffer collisions, and the photocurrent saturates at a low voltage (< 20V) – i.e. at fixed flux of light, increasing the voltage between the electrodes does not increase the collected charge and the current through the tube. In a *gas phototube*, Ne or Ar at low pressure is introduced to amplify the photocurrent. The

gas amplification process is the same as in a gas-filled wire chamber, but the initial electrons now originate not from ionizing gas atoms, but from cathode surface photoemission. Such a device is thus much better suited for detecting radiation at a wavelength that has very low absorption in a gas. As a typical current-voltage behaviour, the photocurrent initially saturates as in a vacuum phototube, but above 20 V it begins to increase, and may be multiplied by a factor of 7 at 80 V.

In *vacuum phototubes*, electrons travel from cathode to anode very quickly, since no collisions occur = short charge collection time. In gas phototubes, the collisions limit the drift velocity of the electrons and ions that are created in the gas, and the charge collection time is much larger.

The photocathode configuration can be such that the photoelectrons are emitted from a metal surface which the light illuminates (*reflection mode*). Alternatively in *transmission mode*, the light first penetrates a thin window of glass or other material, which is coated on the back side by a thin film of photoemissive material in which the light absorbs, so that the photoelectrons are emitted in the same direction as the incoming light.

The quantum efficiency of photocathodes depends strongly on the wavelength of the radiation, for most cathode materials Q.E. peaks at the visible or UV range (Figure 30). Metallic photocathodes and semiconductor photocathodes are the most popular types. Semiconductor cathodes have higher quantum efficiency (QE) but shorter lifetime than metallic cathodes. For example, GaAs has the QE more than 10%, but almost all of the semiconductor photocathodes are extremely sensitive to the contamination, and the working condition for them is high vacuum better than 10^{-6} Pa.

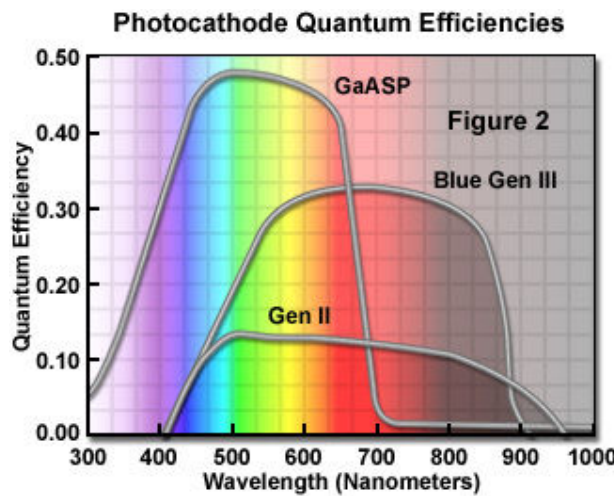


Figure 30. Quantum efficiency of some modern proprietary photocathode formulas [Hamamatsu Photonics, <http://learn.hamamatsu.com/articles/proximity.html>]

Below are given the properties and uses of some common photocathode materials [Hamamatsu Photonics]:

1. Ag-O-Cs. The transmission-mode photocathode using this material is designated S-1 and sensitive from the range of visible light to infrared radiation (300 nm to 1000 nm). The reflection mode covers a slightly narrower range from 300 nm to 1100 nm. This was the first compound photocathode material, developed in 1929.
2. GaAs. GaAs activated in cesium is also used as a photocathode. The spectral response of this photocathode material usually covers a wider spectral response range than multialkali, from ultraviolet to 930 nm, which is comparatively flat over the range between 300 nm and 850 nm.
3. InGaAs. This photocathode material has greater extended sensitivity in the infrared range than GaAs. Moreover, in the range between 900 nm and 1000 nm, InGaAs has a much higher signal/noise ratio than Ag-O-Cs. Some photocathodes can operate at 1700nm.
4. Sb-Cs. Sb-Cs has a spectral response in the ultraviolet to visible range and is mainly used in reflection-mode photocathodes.
5. Bialkali (Sb-Rb-Cs, Sb-K-Cs). These materials have a spectral response range similar to the Sb-Cs photocathode, but have higher sensitivity and lower dark current than Sb-Cs. They also have a blue sensitivity index matching the scintillation flashes of NaI scintillators and so are frequently used for radiation measurement using scintillation counting.
6. High temperature bialkali or low noise bialkali (Na-K-Sb). This is particularly useful at higher operating temperatures since it can withstand up to 175 °C. At room temperatures, this photocathode operates with very low dark current, making it ideal for use in photon counting applications.
7. Multialkali (Na-K-Sb-Cs). The multialkali photocathode has a high, wide spectral response from the ultraviolet to near infrared region. It is widely used for broad-band spectrophotometers and photon counting applications. The long wavelength response can be extended to 930 nm by a special photocathode activation processing.
8. Cs-Te, Cs-I. These materials are sensitive to vacuum UV and UV rays but not to visible light and are therefore referred to as solar blind. Cs-Te is quite insensitive to wavelengths longer than 320 nm, and Cs-I to those longer than 200 nm.

The light also has to penetrate the housing of the detector to reach the cathode. A special window is usually built into the housing that is transparent to the desired range of wavelengths. Particularly for UV-range, materials such as sapphire or modified glasses must be used (Figure 31). The final Q.E.

of a PMT device is then the combination of the Q.E. of the cathode material and the transmittance of the window.

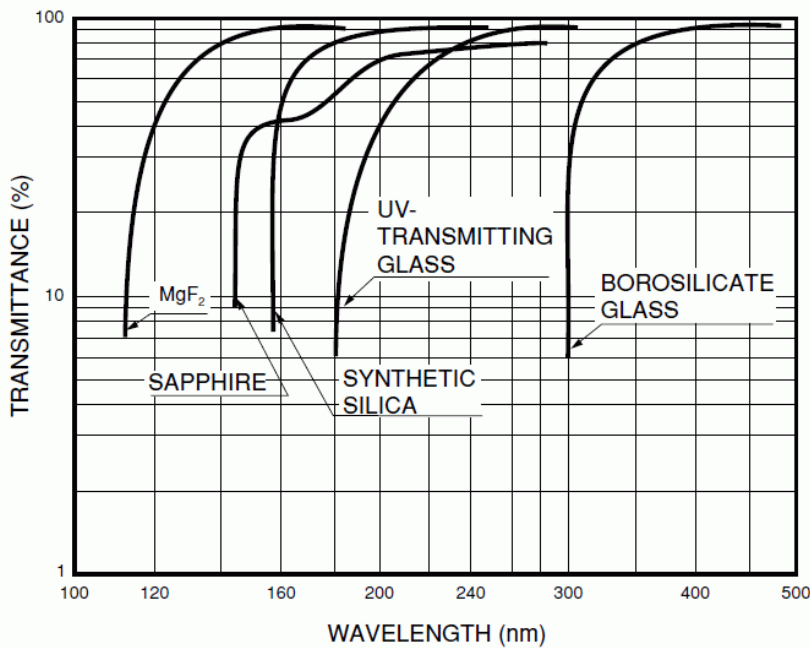


Figure 31. Transmittances of some common window materials used in PMTs [PMT Handbook, Hamamatsu Photonics].

5.2 Photomultiplier tubes

5.2.1 Principle

The major drawback of the simple phototube is its very low gain, making it unsuitable for single particle counting of low flux applications. The solution was developed in the form of a photomultiplier tube (PMT). PMTs are similar to phototubes. They consist of a photocathode and a series of dynodes in an evacuated glass enclosure (Figure 32). Most phototubes contain 10 to 14 dynode stages. Photons that strike the cathode emit electrons due to the photoelectric effect. Instead of collecting these few electrons directly like in the phototubes, the electrons are accelerated towards a series of additional electrodes called **dynodes**, that are each maintained at a more positive potential. Accelerated electrons hit the dynode surfaces, releasing secondary electrons by scattering on atoms. There are several dynodes, creating a cascade effect so that 10^5 to 10^7 electrons are finally released per each photon, depending on the number of dynodes and the accelerating voltage. This amplified signal is collected at the anode.

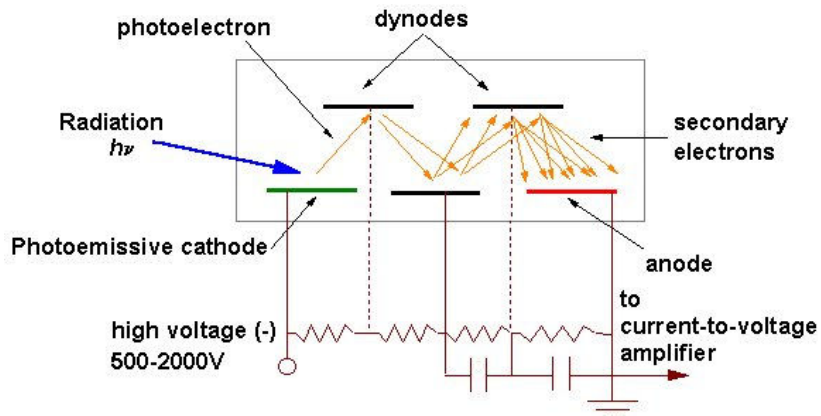


Figure 32 Principle of a PMT.

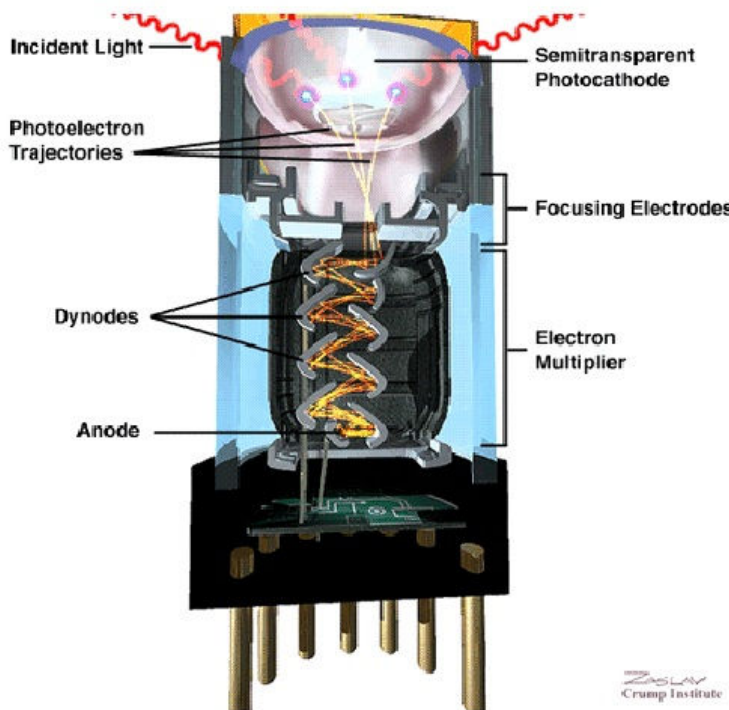


Figure 33. Example of a PMT tube.



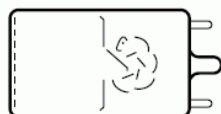
Figure 34. Various PMT designs.

There are many arrangements of dynodes possible for PMTs:

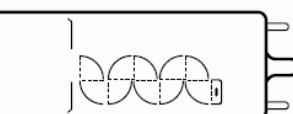
1. Venetian blind
2. Box and Grid
3. Linear focused
4. Circular-cage



(1) Circular-cage Type



(2) Box-and-grid Type



(3) Linear-focused Type



(4) Venetian Blind Type

Figure 35. Configurations of PMTs [PMT Handbook, Hamamatsu Photonics].

5.2.2 Electron-Optical Input System

After electrons are ejected from the photocathode, they must be focussed onto the first dynode stage of the electron multiplication system. This task is performed by the electron-optical input system. In many PMTs, this system consists of electrodes placed in a configuration so that their electric field both collects and focusses the photoelectrons. The figure below shows a schematic diagram of a typical system.

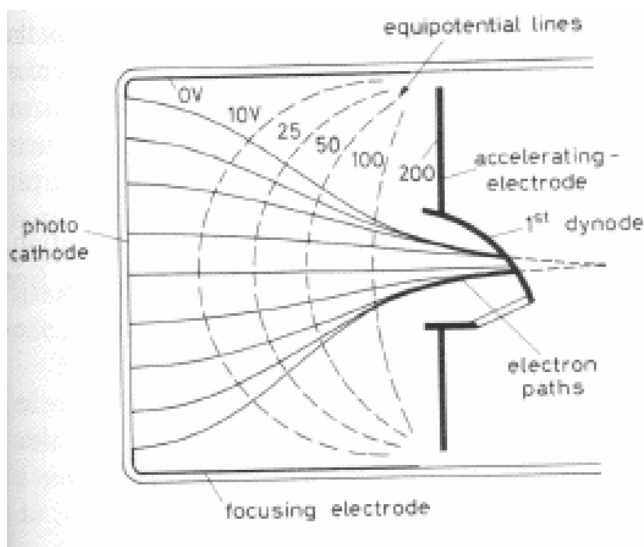


Figure 36. Focussing of electrons in a PMT.

5.2.3 Gain

The secondary electron emission is multiplied by the gain at each dynode stage, called the **secondary emission factor δ** . The electric field between the dynode stages both accelerates and guides the electrons along the multiplier. A dynode consists of a secondary emission material deposited on a conducting material. The surface material should have low work function, so that the energy needed to emit an electron is small and one electron hitting the surface can release more secondary electrons. Secondary emission factors for some dynode materials are shown in Figure 37.

A common technique is to form an alloy of an alkali or alkaline earth metal with a noble metal. During the mixing process, only the alkaline metal oxidizes, so a thin insulating coating is formed on a conducting support. Materials in common use are Ag-Mg, Cu-Be, and Cs-Sb. Some new materials, such as gallium phosphide heavily doped with zinc and a small quantity of cesium, have a negative affinity for electrons – their work function is negative. The secondary emission factor of a dynode made from this material is greatly increased so that fewer stages are needed. This makes for

smaller phototube assemblies and smaller time fluctuations for the signals (hence better time resolution) since the cascade path for electrons is shorter.

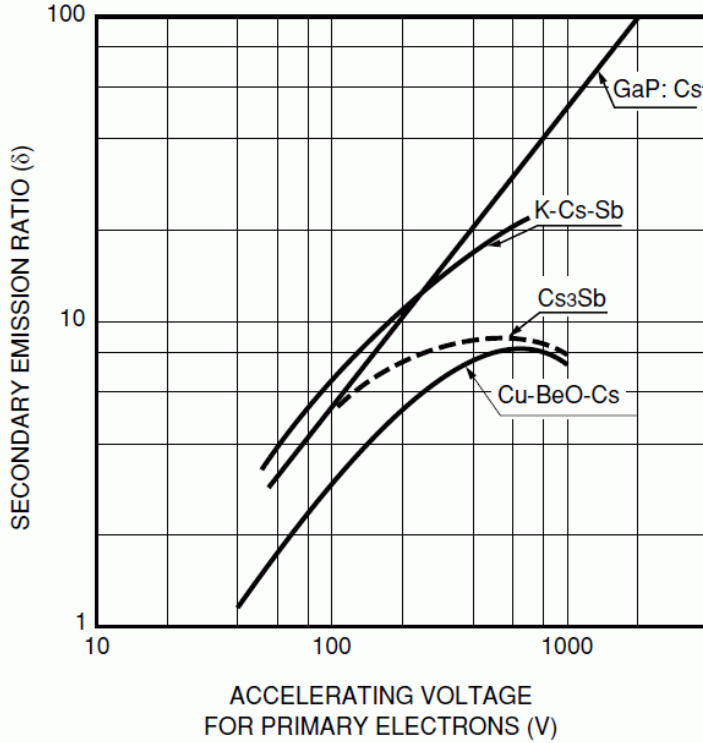


Figure 37. Secondary emission ratios of dynode materials [PMT Handbook, Hamamatsu Photonics]

The overall gain of a phototube depends on the number of dynodes in the multiplier section and their secondary emission factors. To make a quantitative estimate of the gain G , we note that the secondary emission factor is roughly proportional to the voltage V_d between stages,

$$\delta = KV_d \quad (5-1)$$

where K is a constant. (the accurate dependency is $\delta = KV_d^m$, $m = 0.8...0.9$). Assuming the voltage is applied equally to all dynodes, the gain is

$$G = \delta^n \quad (5-2)$$

For a given total voltage difference between the cathode and anode and for a desired gain, there is an optimum number of dynode stages, which can be calculated (*ref. excercises*) as:

$$n = \ln G \quad (5-3)$$

Generally, one wants to minimize the supply voltage to minimize noise, however, if a smaller time spread is needed, larger voltages are beneficial. An important consideration is the variation in gain with supply voltage. This can be calculated from (5-2) and (5-1) as follows

$$\frac{dG}{G} = n \frac{dV_d}{V_d} \quad (5-4)$$

For a 10-stage device, this implies a 10% change in gain for a 1% change in supply voltage. Voltage supplies are generally regulated to better than 0.05%.

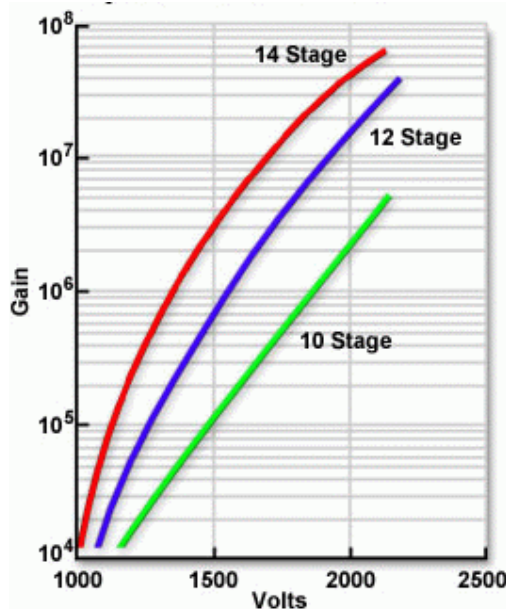


Figure 38. Gain of PMTs vs. anode-cathode voltage.

5.2.4 Time structure

The time resolution of a PMT is affected principally by variations in the transit time of electrons through the photomultiplier and fluctuations in current due to statistical noise. The transit time variations can arise due to differences in the path length traveled by electrons from the photocathode and by variations in the energy with which they are emitted by the photocathode. Electrons on the central axis of the cathode reach the beginning stage dynode before electrons from the edges if they have the same energy simply because the path length is about 3X shorter along the central axis than from the edge. In addition, if electrons are emitted with different energies or different initial directions, then their speed components parallel to the central axis will be different as well.

The transit time spread (TTS) can, at worst, be comparable to the transit time of electrons through the entire tube along the central axis. To reduce the spread, the electric field is increased near the

outer edges of the photocathode so as to accelerate photoelectrons from there to a higher speed than those from the center. Thus, fast phototubes may have adjustable voltages for the focusing and accelerating electrodes in the electron-optical input system part of the phototube.

Table 3. Timing properties of pulses from different types of PMTs (in ns).

Dynode Type	Rise Time	Fall Time	Pulse Width (FWHM)	Electron Transit Time	Unit : ns
Linear-focused	0.7 to 3	1 to 10	1.3 to 5	16 to 50	0.37 to 1.1
Circular-cage	3.4	10	7	31	3.6
Box-and-grid	to 7	25	13 to 20	57 to 70	Less than 10
Venetian blind	to 7	25	25	60	Less than 10
Fine mesh	2.5 to 2.7	4 to 6	5	15	Less than 0.45
Metal channel	0.65 to 1.5	1 to 3	1.5 to 3	4.7 to 8.8	0.4

5.2.5 Noise

Even when no photons are reaching the photocathode, a small current, s.c **dark current** will flow. Dark current sets a lower limit to phototube sensitivity to low light levels. To distinguish a light signal above the background dark current, the photoelectric cathode current must exceed the dark current. In general, dark currents in phototubes should be less than a few nA. The main sources of the dark current are:

1. Thermal emission from the cathode and dynodes: Thermal noise is the principal component in dark current. This contribution is described by Richardson's equation:

$$I = AT^2 \exp\left(-\frac{\Phi}{kT}\right) \quad (5-5)$$

where A is a constant, Φ work function, T temperature, and k is Boltzmann's constant. Lower temperatures lead to a rapid lowering of the thermal current.

2. Leakage currents: leakage current which go through the electrode supports and the pins on the phototube base also contribute to the dark current. The only means of reducing this contribution is to operate the phototube under reduced atmospheric pressure so that the breakdown voltage is lowered.

3. Radioactive contamination in the glass: radioactive materials in the glass housing or support materials of the phototube also produce ionizing particles which can cause electron emission from the photocathodes or dynodes. The radioactivity can also produce fluorescence in the glass housing, thereby contributing light which, in turn, produces dark current.

Afterpulsing: the PMT should be under high vacuum in order to preserve the photocathode material and to minimize gas ionization. Gas ions are drawn back towards cathode or dynodes and can in turn release electrons. This results in **afterpulsing**: pulses occurring after the main pulse of cascaded electrons. The time of the afterpulse is given by the time needed for ions to transit the tube. Under high current, the last stage dynodes can also emit electrode glow which travels back to the photocathode and initiates another shower of electrons.

The light falling on the photocathode material is quantized, consisting of individual photons. The number of counted photons/sec, N , is thus subject to statistical fluctuations. According to Poisson distribution, the standard deviation is then $\sigma = \sqrt{N}$, and we expect the photon count to vary according to this distribution from a measurement (“shot”) to measurement. The same variations are seen when measuring the photocurrent, which is proportional to N (Figure 39). These variations are very general in particle detection and are referred to as **shot noise** or **Schottky effect**.

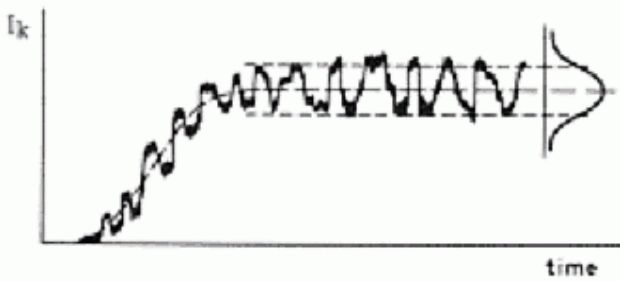


Figure 39. Shot noise in PMT current.

Another source of variations in the photocurrent arises from the electronic circuits due to the random thermal noise present in any resistor R , the **Johnson noise**.

5.2.6 Current and pulse mode operation

PMT is a very sensitive device, that can be used for single photon detection as well as for measuring relatively high fluxes of photons. The output from PMT is treated differently depending on the application:

- DC-method: suitable for high flux when pulses from individual photons merge together, fluctuations in DC current from anode are mostly statistical (Figure 39).
- AC-method: only AC-component of the current is extracted via an RC-filter. Suitable for modulated or low intensity light.

- c) Single photon counting: after extraction and amplification, the pulses are shaped for discrete counting.

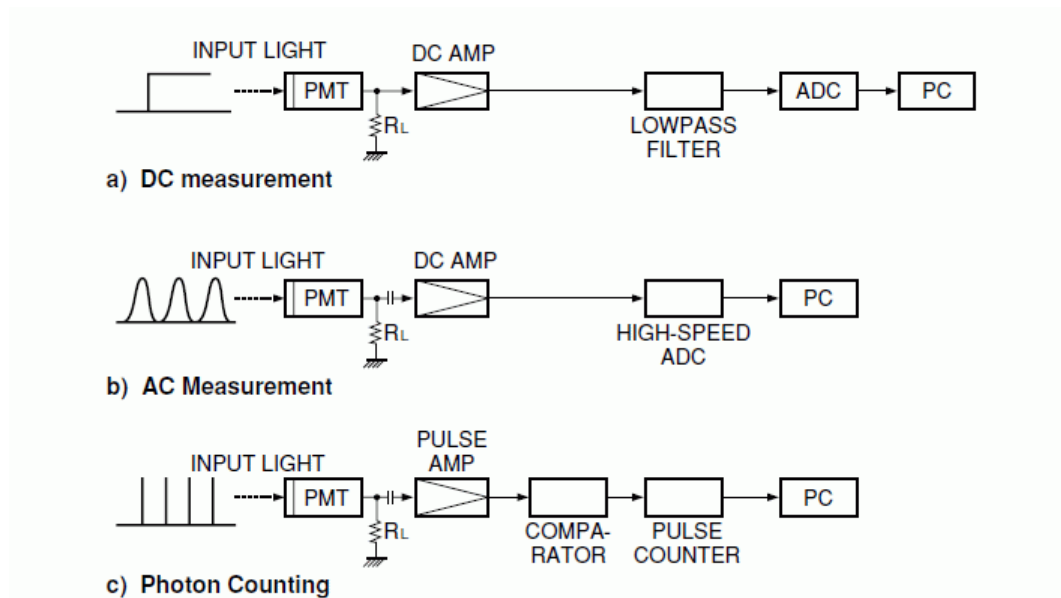


Figure 40. PMT electronic circuitss [http://learn.hamamatsu.com/articles/proximity.html].

When counting single pulses, their height is usually compared with a minimum value – the *lower discriminator level* in a comparator or discriminator and only high enough pulses are passed to the counter. This allows to remove false signals due to dark current or electronic noise. Sometimes also a *high discriminator level* is applied, removing too high pulses. These might be due to very high energy cosmic rays, for example.

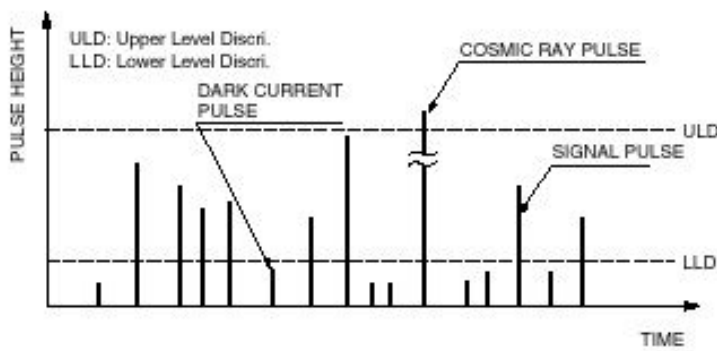


Figure 41. Discriminating of detector pulses.

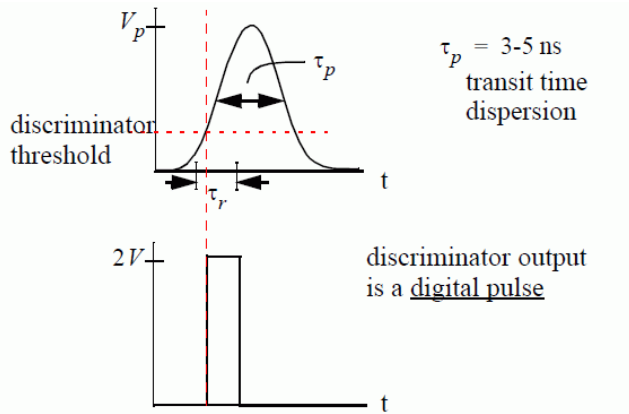


Figure 42. Pulse discrimination for digital counting.

5.3 Channeltrons

Channeltrons® or channel electron multipliers function by exactly the same principle as the PMT's, but the cathode and discrete dynode stages are replaced by a curved tube with the inner surface coated with a high resistance material, along which a potential difference is created – the anode end has positive bias relative to the front end. The coating acts as both the photocathode and secondary electron emitter.

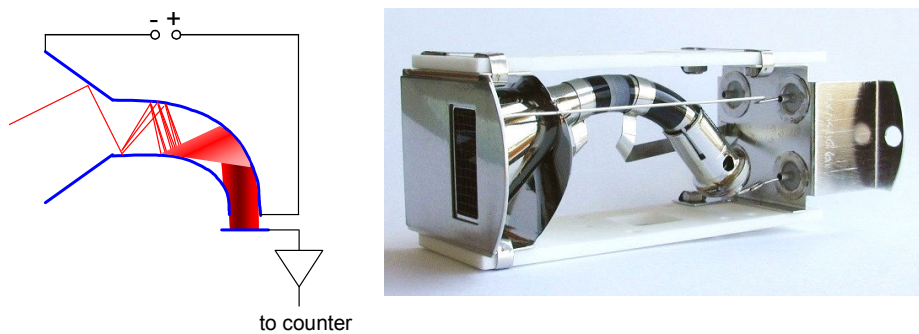


Figure 43. Channeltron® detector.

The photons hit the broader funnel-like portion, emitting photoelectrons, which are accelerated into the tube by the electric field. The curved shape of the tube ensures that before arriving on the anode, the electrons undergo a number of collisions with the tube wall, each time releasing a cascade of secondary electrons.

Channeltrons are normally not encapsulated into a glass enclosure, they are open devices that must be operated in vacuum. They are suitable for detecting photons in a wide wavelength range (Figure 44), but also electrons and ions and are more compact and rugged than PMTs. Their gain is in the range from 10^4 to 10^8 .

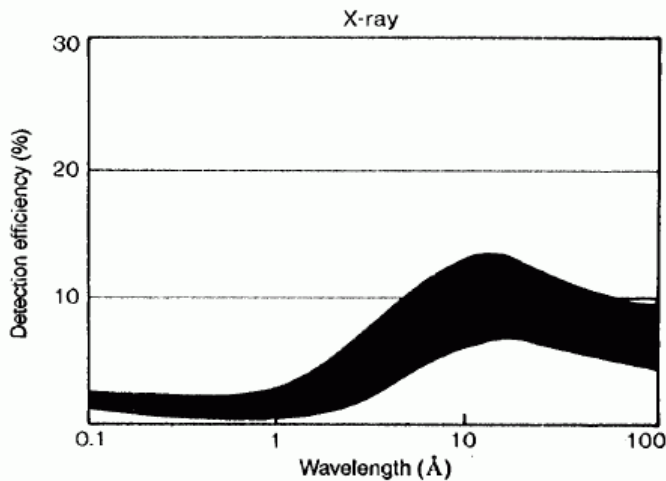


Figure 44. Channeltron Q.E. as a function of photon wavelength [CHANNELTRON ELECTRON MULTIPLIER HANDBOOK, Burle Industries, Inc.]

5.4 Microchannel plates

Microchannel plates (MCPs) are arrays of miniature channeltrons fused together into a thin plate. The arrays consist of minuature coated glass capillaries 10-25 μm diameter and about 1 mm long. The sides of the MCP act as electrodes and the bias voltage, accelerating the electrons though the capillaries, is applied between the sides. The gain of a single plate is 10^3 - 10^4 , the plates are often used in double or triple stack configuration, for a total gain of $>10^6$. To increase the number of times the electrons hit the surface of the capillaries, they can be made at an angle of 7-15 degrees from the surface normal.

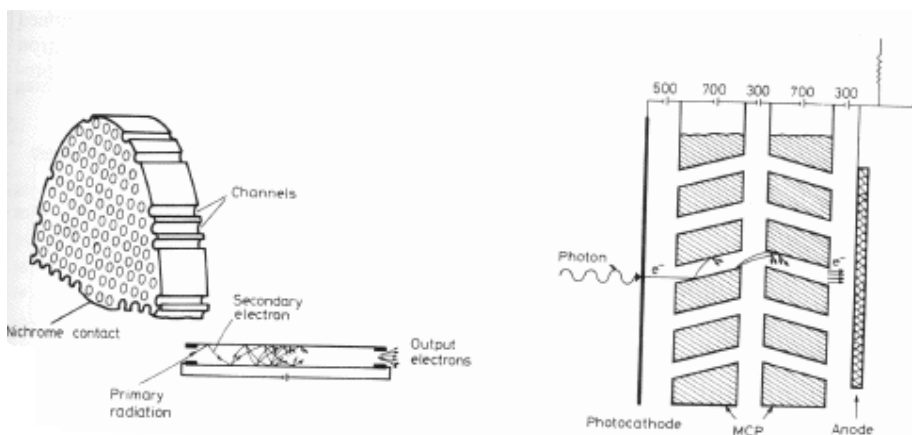


Figure 45. Microchannel plate and its use in a double-stack configuration.

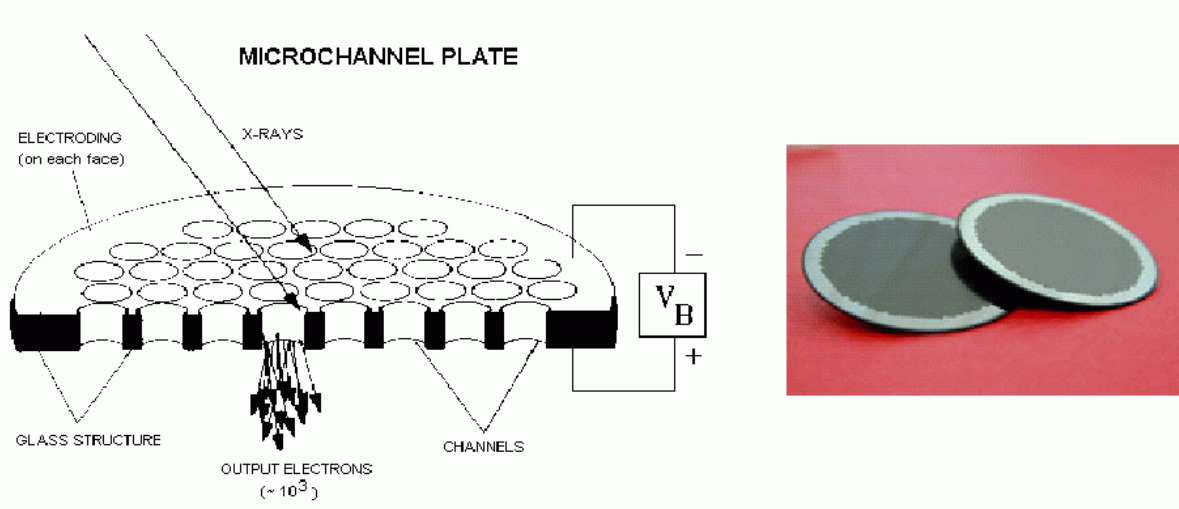


Figure 46. Microchannel plates.

The channel matrix is usually fabricated from a lead glass, treated in such a way as to optimize the secondary emission characteristics of each channel and to render the channel walls semiconducting so as to allow charge replenishment from an external voltage source. Parallel electrical contact to each channel is provided by the deposition of a metallic coating, usually Nichrome or Inconel, on the front and rear surfaces of the MCP, which then serve as input and output electrodes. The total resistance between electrodes is on the order of $10\text{ M}\Omega$. The MCPs have fast charge collection time ($< 100\text{ ps}$) and spatial resolution limited only by the channel dimensions and spacings. Originally developed as an amplification element for image intensification devices, MCPs also have direct sensitivity to charged particles and energetic photons.

5.5 Scintillation detectors

As seen from Figure 30, the Q.E. of photocathode materials falls rapidly towards shorter wavelengths of radiation. Therefore, PMTs are not directly suitable for detecting x-rays and γ -rays. Instead, the radiation must be first converted into the visible range, using the phenomenon of fluorescence (see Section 2.4). For this purpose, a layer of **scintillating material** is placed in front of the photocathode window (Figure 47). Gamma- or x-ray photon interacting with a scintillator produces a pulse of visible light, which is converted to an electric pulse by the photomultiplier tube.

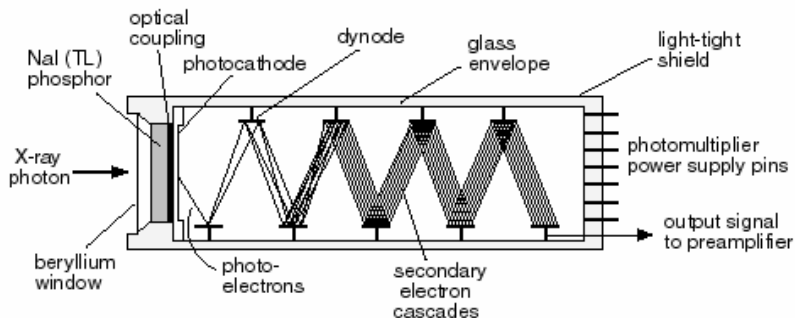


Figure 47. A scintillation detector.

All scintillator materials convert part of the deposited energy into nonradiative form (heat), but using different processes. There are two classes of scintillating materials:

1) Organic scintillators: Molecules in which unlocalized π -type molecular orbitals formed along a benzene ring structure. A common such organic scintillator is anthracene (Figure 48).

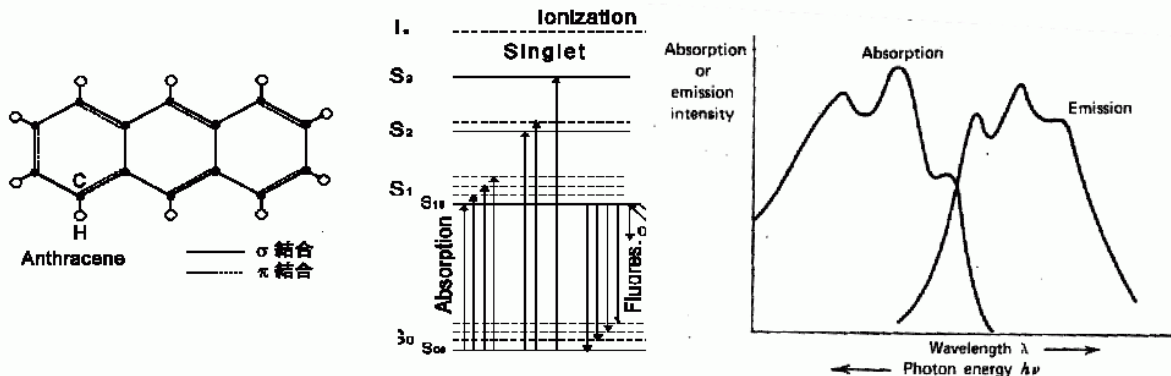


Figure 48. Anthracene molecule; electronic transitions; absorption and emission spectra.

Absorption of incident light excites the π -electrons from the S_{00} ground state to higher quantum states (S_{1n}), which then relaxes to a lower energy level (S_{10}) by dissipating energy to molecular vibrations. The level S_{10} then decays by fluorescence to the S_{0n} levels.

There are many types of organic scintillating materials, usually in the form of plastics, but also liquids or crystals. The organic materials have a fast fluorescence response (2-30 ns) that makes them suitable for timing applications and high rate x-ray counting.

2) Inorganic scintillators: Insulating crystals with large band gap (NaI, CsI), doped with *activators* (Thallium, Cerium) to create impurity levels within the band gap.

- Incident radiation creates electron-hole pairs (excitons) across the band gap.
- Excitons migrate in crystals, become trapped at activatro sites.

- Excitons loose energy to crystal vibrations, populate excited activator energy levels within the band gap.
- Excited state decays to the ground activator level through fluorescence.

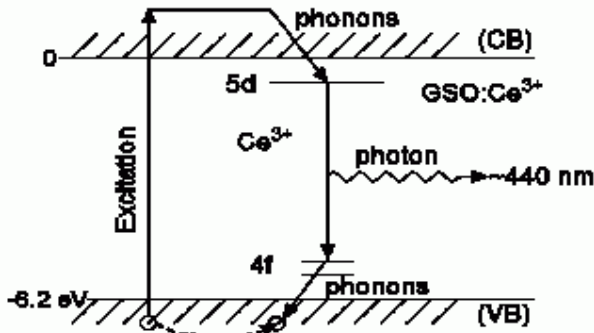


Figure 49. An example of Ce activator-induced fluorescence in inorganic solids

NaI is a very commonly used material, since high Z of iodine in NaI gives high absorption for x- and gamma rays. A small amount of Tl is added in order to activate the crystal. The number of fluorescence photons emitted in NaI (and most other inorganic scintillators) is proportional to the energy of the incoming gamma-ray or x-ray photon. Therefore NaI detectors are suitable for particle energy determination, if the pulse height from the PMT tube is measured (Figure 40, AC-mode). The fluorescence decay time constant in NaI is about 0.25 μ s. For this reason, NaI scintillators are not as well suited as plastic detectors for timing applications or high rate single particle counting.

5.6 Position sensitive detection with MCPs

The narrow capillary structure of MCPs ensures very good output charge localization, corresponding to the spot of arrival of the primary particle. This, and the possibility to fabricate them with large and uniform surface area makes MCP a good basis for position-sensitive detection systems. There are several choices for position readout from the anode:

1) CCD camera detector: a glass anode plate behind MCP is coated with fluorescent material, on which the electron avalanches create spots of visible light. These are recorded and their position digitized using a CCD video camera. Can detect a large number of hits simultaneously, but the update rate of the detector image is slow ($\sim 1/30$ s), as it is determined by the frame rate of the video camera.

2) Resistive anode detector (RAD): the anode plate behind MCP is uniformly coated with a resistive material. The charge released in the MCP is collected from the four corners of the anode and by comparing the pulse heights (~charge) at the four corners, the position on the surface, from

where the pulse originated, can be determined. If the pulse heights measured at the corners are A,B,C,D (Figure 50), then

$$X = \frac{A+D}{A+B+C+D}, \quad Y = \frac{A+B}{A+B+C+D}, \quad (5-6)$$

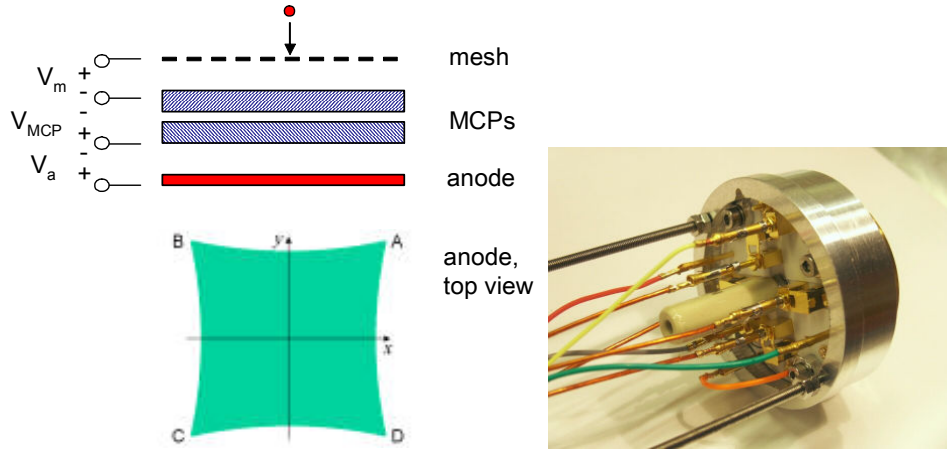


Figure 50. Schematic of the resistive anode detector. Photo – Quantar® Model 3390A.

3) Delay line detector: the anode consists of two coils of thin wire, wrapped in two perpendicular directions. The pulses are collected at both ends of the coils. Since the pulse travels in the coil at a certain velocity, by comparing the arrival times of the pulse at both ends of the coil, the position at which the electrons hit the coil can be determined. One coil gives the x- and the other y-position.

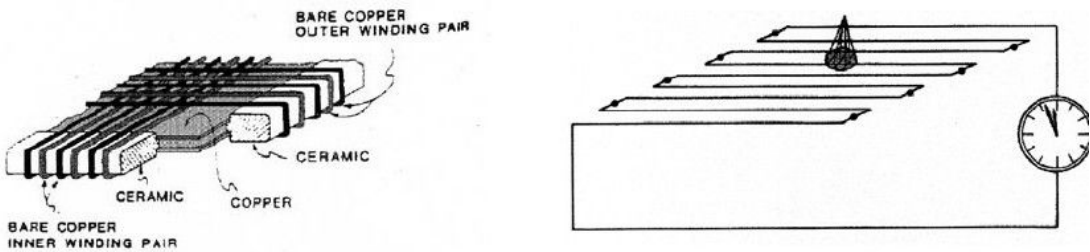


Figure 51. Operating principle of the delay-line detector (Roentdek®).

Types 2) and 3) allow to detect only one electron or ion at a time and detection of the next particle is possible only after a certain dead time. For RAD, this time is typically 2-10 ns. Their advantage is that the coordinates of each hit become available in a timescale of nanoseconds (comp. 1/30 s of CCD detector), which makes them suitable for timing applications.

6 Semiconductor detectors

6.1 Band structure concepts

6.1.1 Electrons and holes

In semiconductors, the band gap E_g is so narrow that although in the ground energy state the conduction band is empty, electrons can easily be excited from the valence band into the conduction band. This also means that both bands are important in terms of electric conductance and one has to deal with the transport of charge carriers in both bands.

To facilitate the discussion of the transport in the "almost-full" valence band of a semiconductor, the concept of **holes** is essential. The holes are "virtual carriers" and it is important to understand that one could deal with only electrons if one is willing to keep track of all the electrons in the valence band. After all, electrons are the only real particles available in a semiconductor, but using the concept of holes, it is easier to keep track of the few missing electrons in an "almost-full" band, rather than keeping track of the huge number of actual electrons in that band. Holes are missing electrons and they carry a positive charge:

$$\begin{aligned} q_h &= +1.602 \times 10^{-19} C; q_e = -1.602 \times 10^{-19} C \\ \vec{k}_h &= -\vec{k}_e \\ E_h(\vec{k}_h) &= -E_e(\vec{k}_e) \\ \vec{v}_h &= \vec{v}_e \\ m_h &= m_e \end{aligned}$$

Let us now consider the currents in a semiconductor in an electric field:

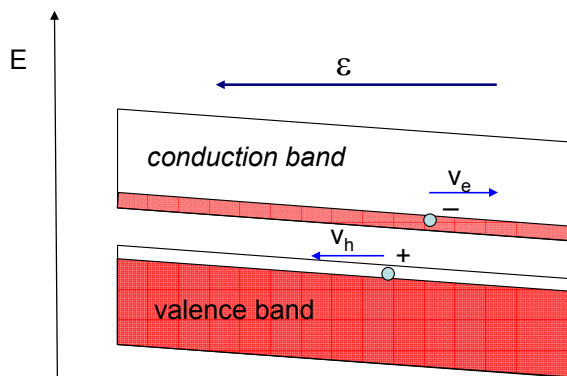


Figure 52. Energy diagram of semiconductor in electric field.

The total current density [A/m^2] has a contribution from both bands (J_v and J_c) and is proportional to the density of occupied electronic states in these bands, N_v^e and N_c^e :

$$J = J_c + J_v; \quad J_c = N_c^e q_e v_e, \quad J_v = N_v^e q_e v_e \quad (6-1)$$

For the valence band, we can express the density of occupied electronic states using the total density of states in the valence band N_v and the density of unoccupied states (holes) N_v^h :

$$J_v = (N_v - N_v^h) q_e v_e \quad (6-2)$$

The first term, sum over all the states has to equal zero since electrons in a completely filled band do not contribute to current. We can thus express the current density in the valence band using the positive hole concept:

$$J_v = -N_v^h q_e v_e = N_v^h q_h v_e \quad (q_h > 0). \quad (6-3)$$

6.1.2 Direct and indirect band gap

The band structure of a solid is described by the function $E(\vec{k})$, the dependency of the energy of quantum states on the momentum vector of the electrons. To show this dependency, $E(k)$ is drawn along certain “cuts” between the points of high symmetry in the 3-dimensional k -space. Such dispersion curves are shown in Figure 54, for example.

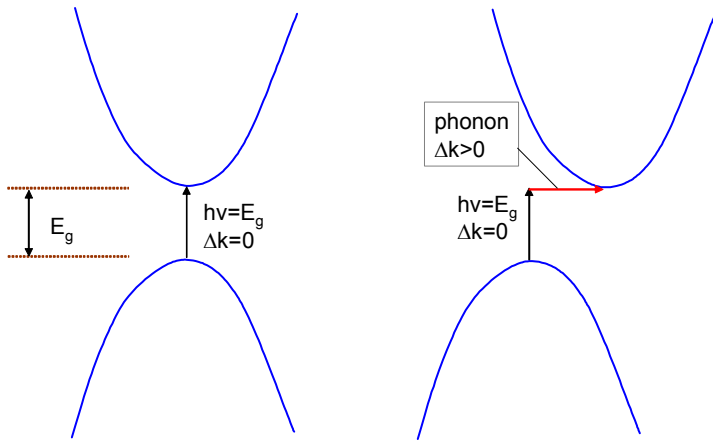


Figure 53. Photoexcitation in a direct and indirect gap semiconductors.

In some cases the top of the valence band lies in a different point of the k -space than the bottom of the conduction band. Such are **indirect gap semiconductors**. If the valence band maximum and conduction band minimum are at the same point, we have a **direct gap semiconductor** (Figure 53). That is an extremely important property in optoelectronic applications. The minimum energy required to excite the electron across the band gap is E_g . When a photon with $h\nu=E_g$ is absorbed by an electron at the top of the valence band, the electron acquires extra energy, but does not change

its momentum \mathbf{k} , since the momentum of the photon is negligibly small. Therefore, electron does not move to a different point along the dispersion curve – a ***vertical transition*** takes place. In a direct gap material, the bottom of the conduction band is indeed reached by the vertical transition, but in an indirect gap material, we need either higher photon energy $h\nu > E_g$ to reach the conduction band vertically, or an additional source to change the momentum of the electron during the transition.

Such a source can be the interaction with the virtual particles of lattice vibrations – ***phonons***. The minimum photon energy that can be absorbed is slightly below the bandgap energy in the case of phonon absorption and has to be slightly above the bandgap energy in the case of phonon emission. Since the absorption process in an indirect bandgap semiconductor involves a phonon in addition to the electron and photon, the probability of having an interaction take place involving all three particles will be lower than a simple electron-photon interaction in a direct bandgap semiconductor. As a result one finds that absorption is much stronger in a direct bandgap material.

Among common semiconductor materials, germanium and silicon have indirect band gaps, but GaAs has a direct band gap.

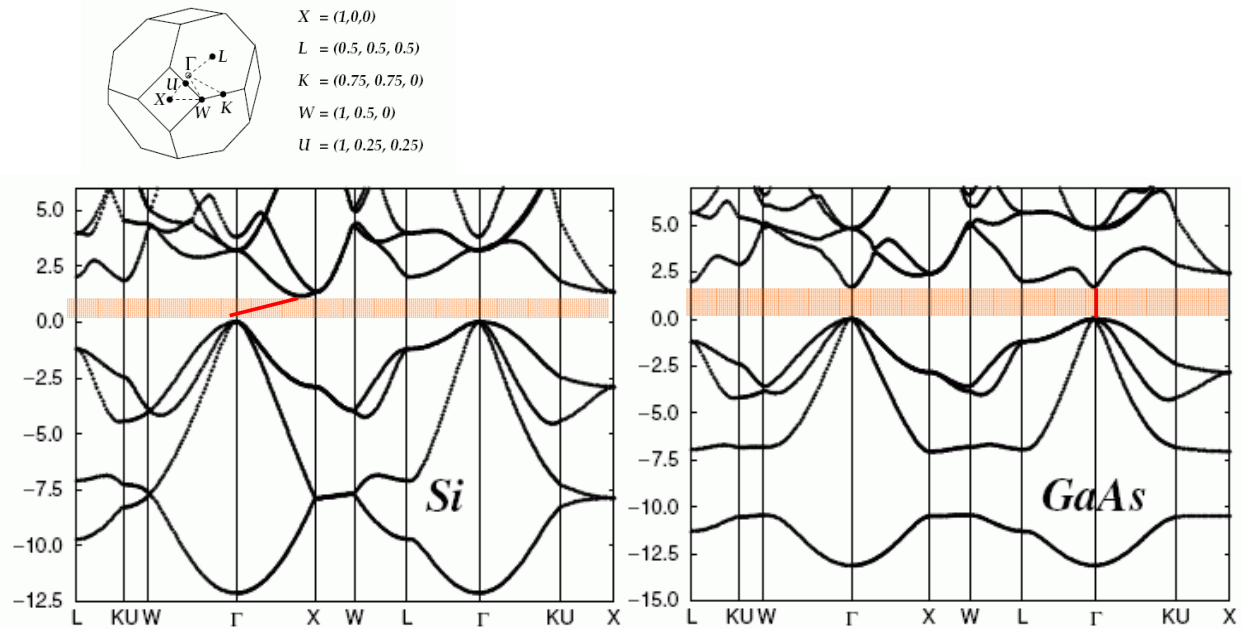


Figure 54. Band structure of Si (indirect gap) and GaAs (direct gap).

GaAs is also by its other properties attractive for optoelectronic applications:

- High electron mobility. This is due to large curvature of the dispersion curve at the bottom of the conduction band \Rightarrow small effective mass m^* .

- Large band gap E_g (1.5 eV or 827 nm).
- Direct band gap.

6.1.3 Effective mass

The effects of the periodic potential in a solid is to destroy the quadratic dispersion, characteristic to the free electrons

$$E(k) = \frac{\hbar^2 k^2}{2m}. \quad (6-4)$$

We can (somewhat artificially) maintain this simple relationship by redefining the mass of the electron so that

$$E(k) = \frac{\hbar^2 k^2}{2m^*}, \quad (6-5)$$

where m^* is the **effective mass**. Instead of using a much more complex form for Eq. (6-5), we “hide” the effects of the lattice in the effective mass. The effective mass is not constant, but depends on \vec{k} . At any point of the dispersion curves we can write:

$$m^* = \frac{\hbar^2}{d^2 E / dk^2} \quad (6-6)$$

This is the definition of the effective mass. In semiconductors, one is usually interested in the top of the valence or bottom of the conduction band. The stronger the curvature of the dispersion curve, the smaller the effective mass. Near the top of the valence band $d^2 E / dk^2 < 0$, so m^* is negative for electrons, but for holes $m^* > 0$ near the maximum of the valence band.

6.2 Intrinsic and doped semiconductors

Intrinsic semiconductors are semiconductors that do not contain impurities. The electron density equals the hole density since the thermal activation of an electron from the valence band to the conduction band yields a free electron in the conduction band as well as a free hole in the valence band.

Doped semiconductors are semiconductors that contain impurities, foreign atoms incorporated into the crystal structure. Either these impurities can be unintentional, due to lack of control during the growth of the semiconductor, or they can be added on purpose to provide free carriers in the semiconductor.

The generation of free carriers requires not only that impurities are present, but also that the impurities give off electrons to the conduction band in which case they are called **donors**. If they give off holes to the valence band, they are called **acceptors**, since they effectively accept an electron from the filled valence band.

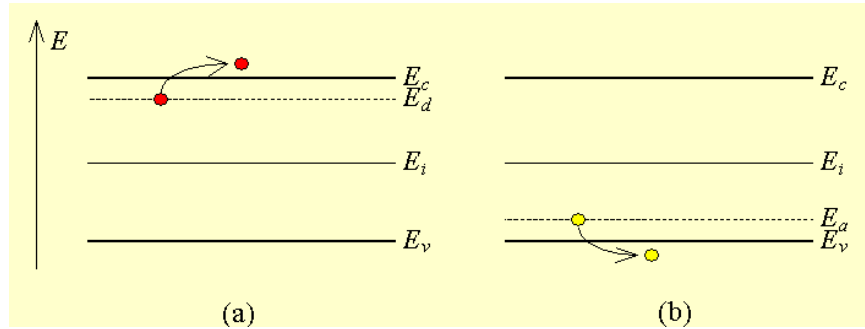


Figure 55 Ionization of a) a shallow donor and b) a shallow acceptor.

A semiconductor doped with impurities that donated or accepted an electron will therefore contain free carriers. *Shallow impurities* require little energy - typically around the thermal energy, kT , or less – to donate or accept electrons. *Deep impurities* require energies much larger than the thermal energy to ionize so that only a fraction of the impurities present in the semiconductor contribute to free carriers. Deep impurities, which are more than five times the thermal energy away from either band edge, are very unlikely to ionize. Such impurities can be effective recombination centers, into which both electrons and holes fall. Such deep impurities are also called *traps*.

- **n-type semiconductors:** donors provide free electrons to the conduction band
- **p-type semiconductors:** acceptors provide free holes to the valence band

6.3 p-n junctions

(based on “Principles of Semiconductor Devices”, B. Van Zeghbroeck, 2004)

p-n junctions consist of two semiconductor regions of opposite type. Such junctions show a pronounced rectifying behavior and are also called p-n diodes in analogy with vacuum diodes.

The p-n junctions can be used as solar cells, photodiodes, light emitting diodes and even laser diodes.

A p-n junction shown in Figure 56 has a p-type region on the left with an acceptor density N_a , while the region on the right is n-type with a donor density N_d . The dopants are assumed to be shallow, so that the electron density in the n-type region is approximately equal to the donor density and the hole density in the p-type region is approximately equal to the acceptor density.

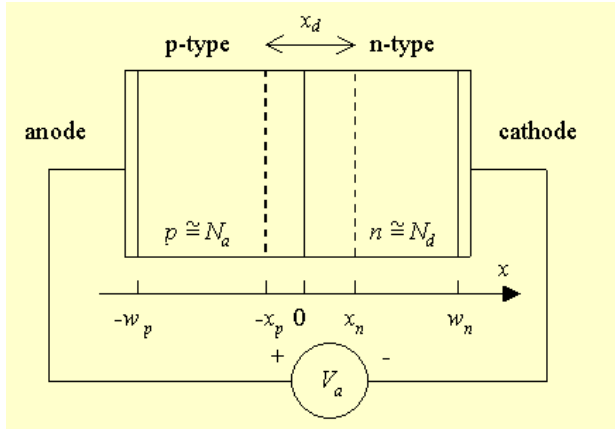


Figure 56. Cross-section of a (forward-biased) p-n junction.

We assume that the doped regions are uniformly doped and that the transition between the two regions is abrupt: an *abrupt p-n junction*.

If one side of the p-n junction is distinctly higher-doped than the other, then only the low-doped region needs to be considered, since it primarily determines the device characteristics: a *one-sided abrupt p-n junction*. A junction is *forward-biased* if a positive voltage is applied to the p-doped region and *reversed-biased* if a negative voltage is applied to the p-doped region.

In order to understand the functioning of p-n junction, let's assume that one can bring both semiconductor regions together, aligning both the conduction and valence band energies of each region. This yields the so-called *flatband diagram*:

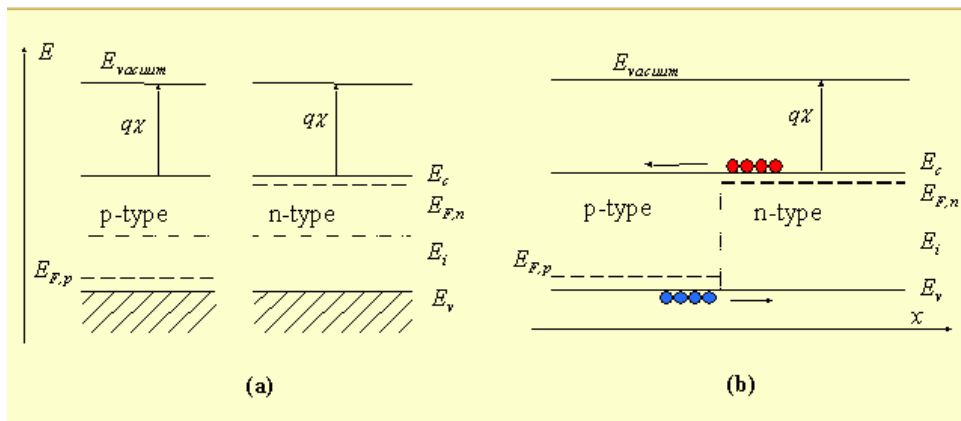


Figure 57. Energy band diagram of a p-n junction (a) before and (b) after merging the n-type and p-type regions.

Note that the Fermi energies, $E_{F,n}$ and $E_{F,p}$ are not aligned. This flatband diagram is not an equilibrium diagram, since both electrons and holes can lower their energy by crossing the junction. A motion of electrons and holes is therefore expected before thermal equilibrium is obtained. To reach thermal equilibrium, where the Fermi energy is constant throughout the material, electrons

(holes) close to the metallurgical junction diffuse across the junction into the *p*-type (*n*-type) region where hardly any conduction electrons (holes) are present. The electrons then recombine with holes in the *p*-region and *v.v.* This process creates a region around the junction, which is depleted of mobile carriers: the ***depletion region***, extending from $x = -x_p$ to $x = x_n$. It leaves the ionized donors (acceptors) behind and their charge causes an electric field, which in turn causes a drift of carriers in the opposite direction. The diffusion of carriers continues until the drift current balances the diffusion current, thereby reaching thermal equilibrium as indicated by a constant Fermi energy across the junction:

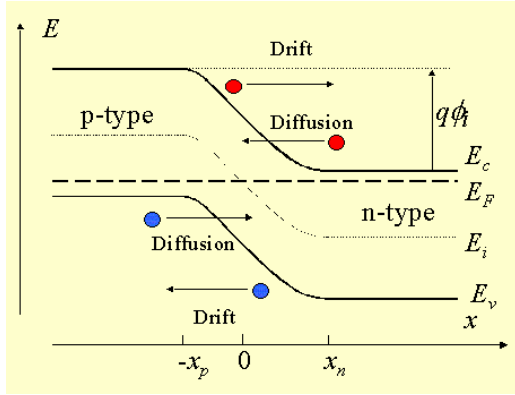


Figure 58. Achieving thermal equilibrium across the p-n junction.

While in thermal equilibrium no external voltage is applied between the *n*-type and *p*-type material, there is an internal potential, the so-called ***built in potential*** ϕ_i [V]. The energy $q\phi_i$ (q -elementary charge) is the shift of the bands, which is just the difference between the Fermi energies of the *n*-region and *p*-region before they came to contact and achieved the thermal equilibrium. The built-in potential provides a barrier, which prevents current flow across the junction, and it's an important characteristic of the junction.

In order to estimate $q\phi_i$, we first relate the distance of the Fermi level from the bottom of the conduction band to the electron density N_c in the conduction band (in the equilibrium):

$$E_c - E_F = k_B T \ln \left(\frac{N_c}{N_d} \right) \quad (6-7)$$

where N_d is the density of donors. Similalry, the distance of the Fermi level from the top of the valence band is related to the concentration of holes:

$$E_F - E_v = k_B T \ln \left(\frac{N_v}{N_a} \right) \quad (6-8)$$

where N_a is the density of acceptors. From Figure 57 and Figure 58 one can see that

$$\begin{aligned} q\phi_i &= E_g - (E_c - E_F) - (E_F - E_v) \\ q\phi_i &= E_g - k_B T \ln \left(\frac{N_c N_v}{N_d N_a} \right) \end{aligned} \quad (6-9)$$

Note that the built-in potential is temperature-dependent.

Example: N_c and N_v are typically about 10^{19} cm^{-3} and it's easy to find semiconductors with dopant densities N_a and $N_d \approx 10^{15} \text{ cm}^{-3}$. With a band gap $E_g = 1 \text{ eV}$, we obtain at room temperature (where $k_B T = 0.025 \text{ eV}$): $q\phi_i = 0.54 \text{ eV}$.

6.3.1 Biased p-n junctions

Let's now consider the changes in the band diagram if a voltage V_a is applied across the junction.

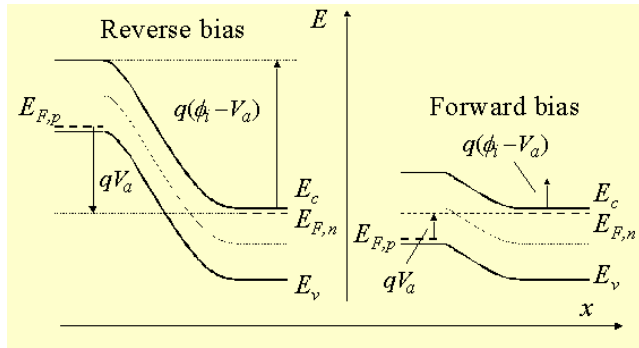


Figure 59. Biased p-n junction.

The total potential across the semiconductor equals the built-in potential minus the applied voltage:

$$\phi = \phi_i - V_a. \quad (6-10)$$

The electric field inside the device now again shifts the Fermi levels of the p- and n-type sides, that became aligned in the thermal equilibrium (Figure 59), away from each other. The shift is equal to qV_a .

Forward bias:

Under *forward bias* (positive voltage to p-region), the electrons on the n-side "see" a lower potential energy barrier than they saw when no voltage was applied. The flow of electrons into the p-side becomes easier. One can track the motion of the electron starting at the negative terminal, moving towards the n-type side of the diode. Having reached the n-type region it enters the conduction band of the semiconductor and makes its way towards the p-n junction. It crosses the barrier easily due to the forward bias (the thin insulating depletion zone produces very little

electrical resistance). Once inside the p-type region, the electron will **recombine** with a hole and fall into the valence band, where it will drift towards the positive terminal of the power supply. This process will be repeated over and over again, producing a complete circuit path through the junction. Electrons drift towards the positive terminal also in the conduction band, this process can be significant if the recombination is slow.

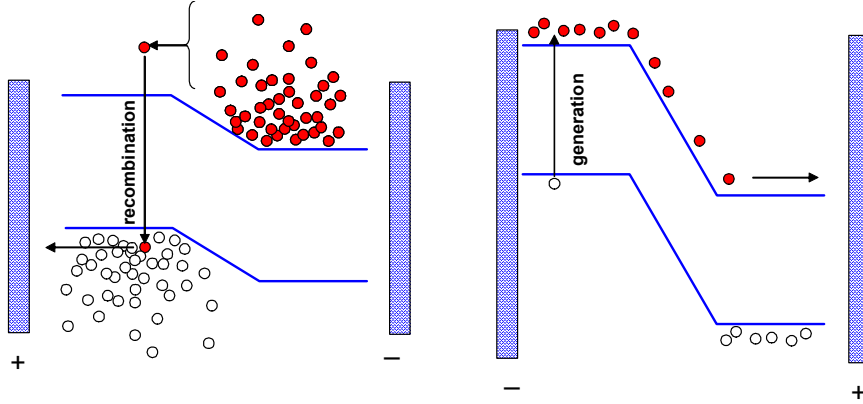


Figure 60. Left: Current in forward-biased p-n junction. Right: Current in reverse-biased p-n junction.

How exactly the current I depends of the applied bias voltage, can be obtained by calculating the density of these electrons in the n-side that can overcome the potential barrier ϕ . The density depends on the concentration of donors and on the temperature through the Fermi-Dirac distribution. We obtain

$$I \propto N_d \left(\exp\left(\frac{qV_a}{k_B T}\right) - 1 \right) \quad (6-11)$$

It is usually given as the **diode equation**

$$I = I_{sat} \left(\exp\left(\frac{qV_a}{k_B T}\right) - 1 \right) \quad (6-12)$$

where I_{sat} is the **saturation current**, typically $\sim 10^{-12}$ A.

Reverse bias:

Under **reverse bias** (negative voltage to p-region), the only current which flows is the reverse saturation current, resulting from the few thermally generated minority carriers which can fall down (or up) the barrier.

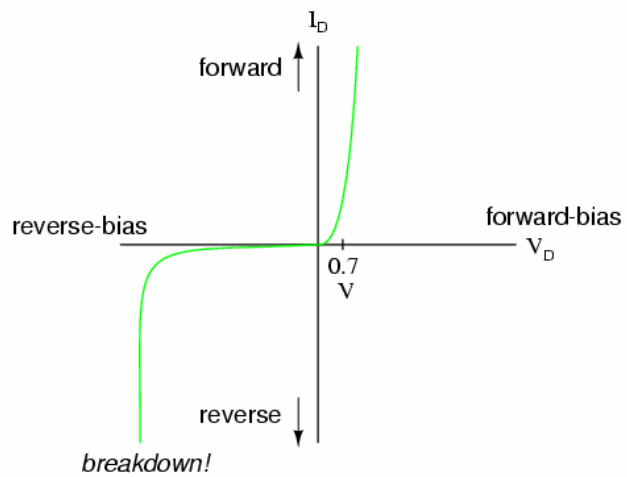
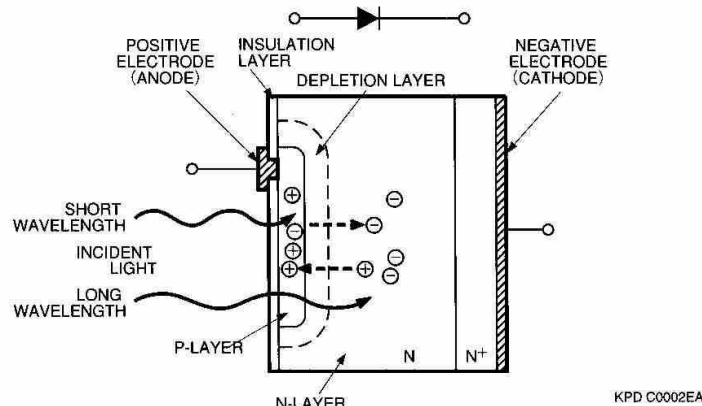


Figure 61. General behaviour of the I-V curve of a p-n junction.

p-n junctions are an integral part of several optoelectronic devices. These include photodiodes, solar cells light emitting diodes (LEDs) and semiconductor lasers.

6.4 Photodiodes and solar cells

6.4.1 Generating photocurrent



(b): Photodiode P-N Junction State

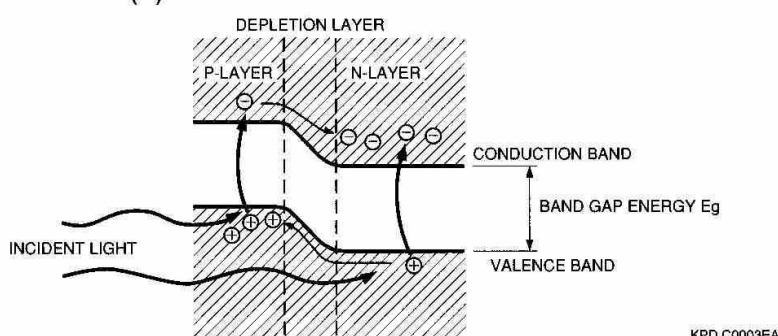


Figure 62. Photodiode and its energy diagram.

Photodiodes and crystalline solar cells are essentially the same as the p-n diodes. Figure 62 shows a cross section of a photodiode. The p-region material at the active surface and the n-region at the substrate form a p-n junction. The events that occur when the diode is illuminated are:

- When the incident light energy is greater than the band gap E_g , the electrons are excited into the conduction band, leaving holes in the valence band. These electron-hole excitations occur throughout the p-region, depletion layer and n-region.
- In the depletion layer, the electric field accelerates these electrons toward the n-region and the holes toward the p-region.
- Of the electron-hole pairs generated in the n-region, the electrons, along with electrons that have arrived from the p-region and depletion zone, are left in the n-region's conduction band. Holes remain in the p-region.
- Holes created in the n-region diffuse through the n-region to the depletion layer, then are pulled into the p-region by the electric field.
- This results in the accumulation of positive charge in the p-region and a negative charge in the n-region.
- If an external circuit is connects the p- and n-regions, electrons will flow through it from the n-region to p-region, where they recombine with holes. This is the **photocurrent I_{ph}** (Figure 63).
- The photocurrent creates a voltage through the external resistor R_L , creating a voltage V_a , so that the diode becomes forward biased and the diode current I_{diode} starts to flow.
- The two opposing currents add up to an equilibrium current I and voltage V_a . The circuit can also include an external voltage source, to bias the diode junction differently than by V_a .

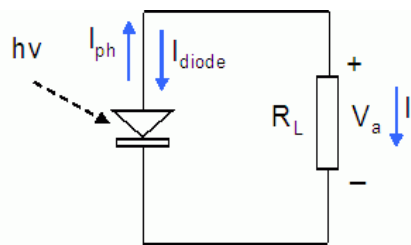


Figure 63. Currents in a photodiode circuit without external voltage source.

The photoexcited electron-hole pairs are most effectively collected from the depletion region, where the possibility of recombination is small and the drift velocity is high.

The total current is given by:

$$I = I_{sat} \left(\exp\left(\frac{qV_a}{k_B T}\right) - 1 \right) - I_{ph} \quad (6-13)$$

The photo-generated carriers thus cause a photocurrent, which opposes the diode current under forward bias. The diode can be used as a **photodetector** - using a reverse or zero bias voltage - as the measured photocurrent is proportional to the incident light intensity.

The diode can also be used as a **solar cell** - using a forward bias - to generate electrical power. The simplest circuit of connecting a solar cell is shown in Figure 63. The sun's spectrum is consistent with that of a black body at a temperature of 5800 K. The radiation spectrum has a peak at $h\nu=0.8$ eV and a significant part of the spectrum is in the visible range of the spectrum (400 - 700 nm). The power density is approximately 100 mW/cm², dependent upon atmospheric scattering and absorption, the season and the latitude of a specific location. Of the solar light, which does reach a solar cell, only photons with energy larger than the energy bandgap of the semiconductor generate electron-hole pairs. In addition, one finds that the voltage across the solar cell at the point where it delivers its maximum power is less than the bandgap energy in electron volts. The overall power-conversion efficiency of single-crystalline solar cells ranges from 10 to 30 % yielding 10 to 30 mW/cm².

The *open-circuit voltage* V_{oc} is defined as the voltage across the illuminated cell at zero current I .

The *short-circuit current* I_{sc} is the current through the illuminated cell if the voltage across the cell is zero.

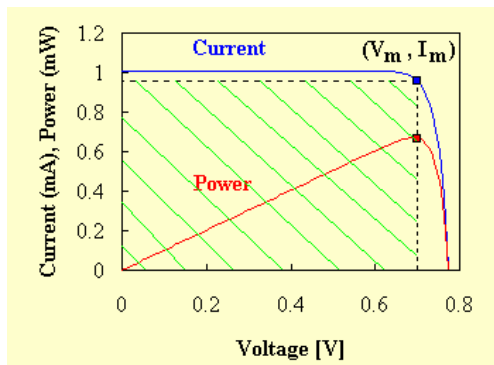


Figure 64. Current-Voltage (I - V) and Power-Voltage (P - V) characteristics of a p-n diode solar cell with $I_{ph} = 1$ mA and $I_s = 10^{-10}$ A. The crosshatched area indicates the power generated by the solar cell.

The short-circuit current is close to the photocurrent while the open-circuit voltage is close to the turn-on voltage of the diode. The power output over the resistance R_L is

$$P_{out} = V_a I \quad (6-14)$$

which is the area of the rectangle extending to a point in the I-V curve (Figure 64). P_{out} increases linearly with the diode voltage but then rapidly goes to zero as the voltage approaches the turn-on voltage of the diode. The maximum power is obtained at a point (V_m, I_m). The efficiency Q of the solar cell is then

$$Q = \frac{V_m I_m}{P_{in}}. \quad (6-15)$$

In designing solar cells with best efficiency, two contracting effects must be taken into account:

- The upper bound for the open circuit voltage V_{oc} is given by the built-in potential: $V_{oc} < q\phi_i$, which is roughly proportional to the energy gap E_g . Thus, large band-gap materials would be more effective.
- Only photons with energies larger than the band gap, $h\nu > E_g$ are absorbed and, hence, the light-generated current decreases with an increase in E_g .

As a consequence of these two factors, the solar cell efficiency is the largest for the energy gap of about **1.4 eV** at room temperature, such as in GaAs, and GaAs-based solar cells.

6.5 Visible and infrared light detectors

6.5.1 Absorption and spectral responsivity

The absorption of a photon produces an electron hole-pair and thus a photocurrent. The absorption of the photons depends on the absorption coefficient α_0 in the medium, which is strongly wavelength dependent. The photocurrent caused by the absorption of photons can be calculated by

$$I_{ph} = N_0 q \times Q.E. = P_0 \frac{q\lambda}{hc} \times Q.E., \quad (6-16)$$

$$Q.E. = (1 - R) [1 - e^{-\alpha_0 d}],$$

where N_0 is the incoming photon flux [s^{-1}], P_0 is the optical power [W], λ is the wavelength of the incident light, h is the Planck constant, and q is the elementary charge. The quantum efficiency Q.E. depends on the reflection at the interface of the detector and air: $(1-R)$ is the light absorbed in the detector, and the exponential term describes the absorption in the medium with the thickness d . The absorption coefficient α_0 strongly depends on the wavelength (Figure 65).

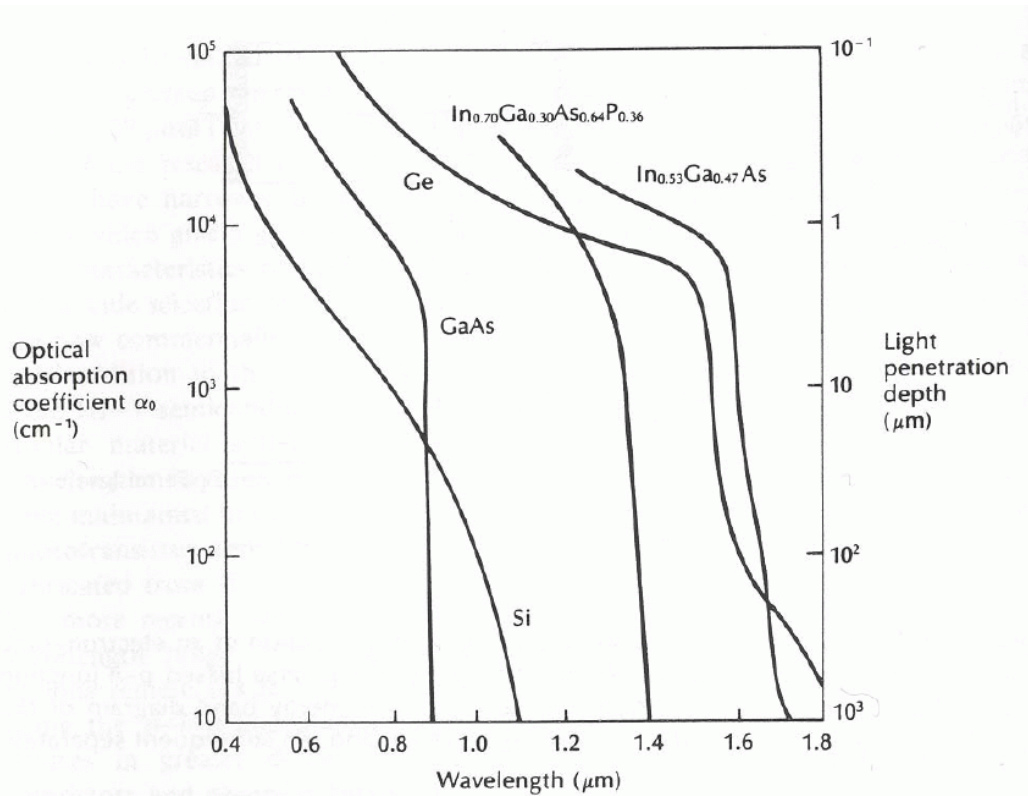


Figure 65. Optical absorption coefficients in semiconductor materials.

When operating in the visible light range, one absorbed photon produces 1 electron-hole pair in the semiconductor. In practice, it means that the detectors are operated in the *current mode*, measuring the total photocurrent generated by a large flux of incoming photons.

Silicon and germanium have direct and indirect optical transitions but the lowest energetic transition is an indirect optical transition. The fact that silicon and germanium are indirect band gap semiconductors leads to the strong wavelength dependent absorption of the material. The direct band gap semiconductors (GaAs) exhibit a very sharp drop in the optical absorption at the photon energy close to the bandgap value.

- In silicon the optical bandgap at room temperature is 1.14eV, which corresponds to a wavelength of 1100 nm. Up to 1100 nm silicon is still absorbing even though the absorption coefficient for wavelength >1000nm is already relatively low. At higher wavelengths Si becomes transparent.
- The optical bandgap of germanium is 0.67eV, which corresponds to a much higher cut-off wavelength of about 1850nm. However, due to the small bandgap the thermal leakage current of germanium diodes is very high, which therefore makes cooling necessary.
- Gallium arsenide has a direct optical bandgap of 1.43eV. In order to increase the absorption in the infrared part of the spectrum, (which is necessary for the optical communication system for example), it is doped with indium, which reduces the bandgap of gallium arsenide (Table 4).

Table 4. Bandgaps of semiconductor materials used for light detection [J.M. Senior, *Optical Fiber*

Communications].

Bandgap (eV) at 300 K		
	Indirect	Direct
Si	1.14	4.10
Ge	0.67	0.81
GaAs	—	1.43
InAs	—	0.35
InP	—	1.35
GaSb	—	0.73
In _{0.53} Ga _{0.47} As	—	0.75
In _{0.14} Ga _{0.86} As	—	1.15
GaAs _{0.88} Sb _{0.12}	—	1.15

The most commonly used characteristic, quantum efficiency, does not take into account the photon energy. For optical detectors operating in a range of wavelength, it is practical to use the **spectral**

responsivity S instead, given by the ratio of the phtotocurrent [Amperes] to the incident optical power [Watts]:

$$S = \frac{I_{ph}}{P_0}. \quad (6-17)$$

The spectral sensitivity relates to the quantum efficiency as

$$S = Q.E. \cdot \frac{q\lambda}{hc} \quad (6-18)$$

The photocurrent of an optical detector should be linear with P_0 . In order to extract almost all photo-generated carriers out of the device a reverse bias voltage can be applied to the diode, increasing the electric field in the depletion region (Figure 59).

6.5.2 Light detector types

Pn-diodes

The basic diode type that was discussed above. The photocurrent arises mainly from the electron-hole pair creation in a relatively narrow depletion region.. A pn-diode(like all other diodes) can be operated under short circuit conditions or under reverse bias voltage. Depending on the used material the quantum efficiency of the diode might be slightly higher at reverse bias voltage and also the charge collection time can be shorter and time resolution better.

The signal to noise ratio of the diode is mainly defined by the used material. The smaller the optical bandgap and the higher the number of electronic defects in the material the higher the leakage current. Since the depletion region is very thin, the Q.E. of a pn-diode is usually not very high. Most of the light that is absorbed will simply not contribute to the overall photocurrent, but the electron-hole pairs will recombine in the n- and p- regions.

pin-diodes

In order to extend the region of carrier extraction an *intrinsic layer* or a slightly doped layer is usually introduced between the p- and the n-region. As a consequence the depletion region is extended across the intrinsic or lightly doped layer and therefore more photo-generated carriers contribute to the photocurrent.

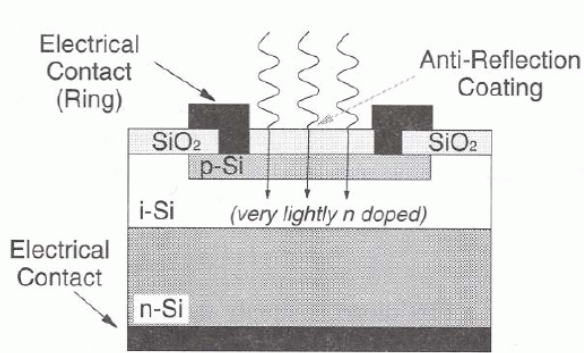


Figure 66. Cross-section of a pin-diode [H. J.R. Dutton, *Understanding optical communications*].

The pin-diode can be realized as an homo-junction or a heterojunction. If the structure is realized in silicon the device will be usually a homojunction. Under such conditions all three layers (p-,i- and n-region) have the same optical bandgap.

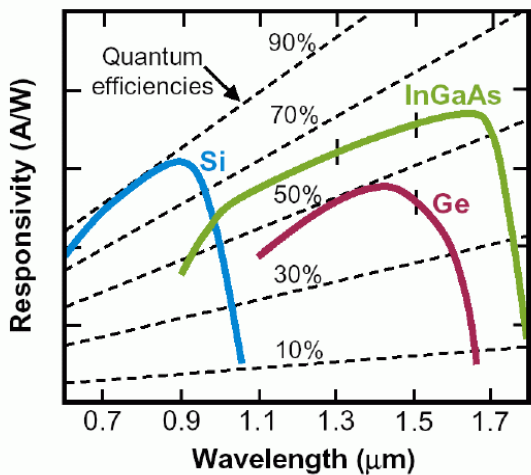


Figure 67. Responsivity and Q.E. of PIN diodes.

Schottky Barrier diodes

The sensitivity of the detector has to be matched with the optical spectrum of the incident light. However, sometimes it is not possible to realize pn-diodes for a given wavelength band. One alternative to overcome this limitation is a Schottky Barrier Diode, where a thin metal layer replaces either the p- or the n-region of the diode. Depending on the semiconductor and the metal being involved a barrier is formed at the interface of the two materials. This barrier leads to a bending of the bands, further modified by the applied voltage. In the region of the band bending the electron hole pairs can be separated, as was done in the depletion region of the pn-diodes.

Avalanche Photodiodes (APD)

One way of increasing the sensitivity of the detector is amplification. The operating principle of a APD is based on the avalanche effect, very similar to what happens in the proportional gas counters, where a highly accelerated electron excites another electron in collisions with the atoms in the medium. The device operation works as following: photons pass through the n+ and p layers and useful photoabsorption takes place in the depletion region (π , Figure 68 and Figure 69) The electric field in the π -region is high enough to separate the carriers, but not high enough for the charge carriers to gain enough energy needed for secondary ionization in collisions. However, in the n+ and p-region boundary is significantly higher so that the electrons are accelerated to such kinetic energy between collisions with the lattice atoms that they start to create new electron-hole pairs in these collisions.

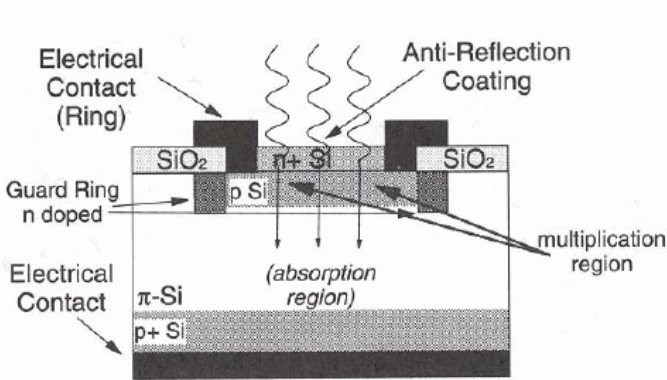


Figure 68. Avalanche photodiode [H.J.R. Dutton, *Understanding optical communications*].

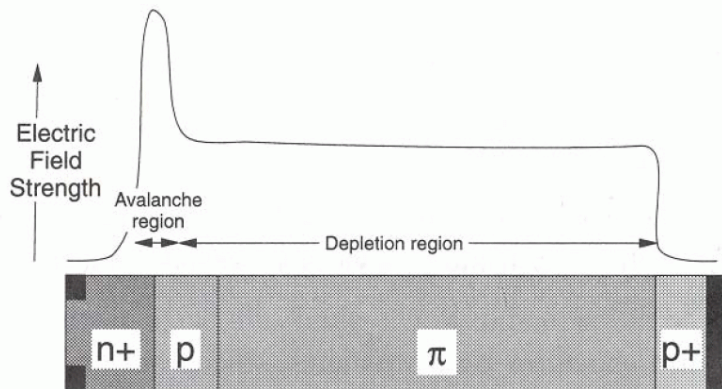


Figure 69. Silicon Avalanche Photodiode (APD) [H.J.R. Dutton, *Understanding optical communications*].

6.6 Semiconductor γ - and x-ray detectors

The types of radiation that can be measured with semiconductor detectors includes a large portion of the electromagnetic spectrum, with photon energies ranging from <1 eV to ~ 10 MeV, and charged particles with energies from keV to GeV.

Contrary to the visible light, an x-ray or g-ray photon creates a large number of electron-hole pairs when absorbed in a semiconductor detector. Figure 70 shows the average energy required for pair creation in different detector materials as a function of the band gap of the material. Compared to gas-filled detectors, the pair-creation energy δ is considerably smaller, and the charge deliberated by a photon with a certain energy would be larger than in gas-filled detectors.

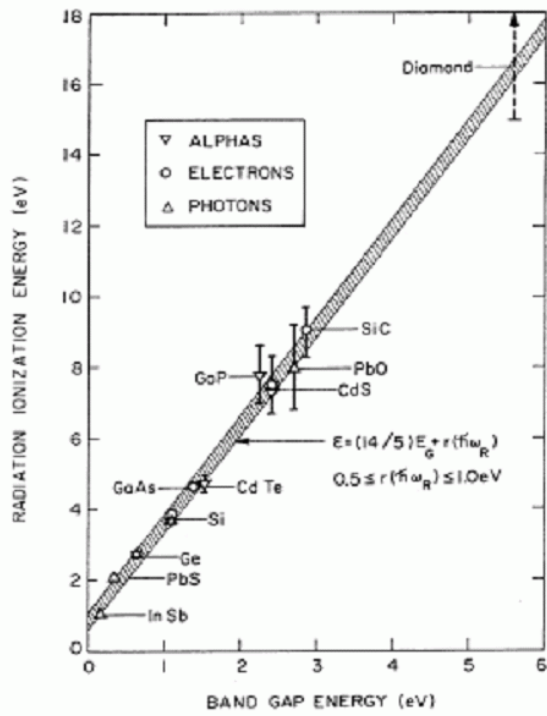


Figure 70. Pair creation energy in semiconductor detectors.

The physical processes themselves, that create the electron-hole pairs, are quite similar to those occurring in a gas – the absorbed quantum releases high-energy photo- and Auger electrons from core levels of an atom in the material. These electrons will gradually lose energy in collisions that create new electron-hole pairs, until the initial energy $h\nu$ is dissipated in average to

$$\bar{n} = \frac{h\nu}{\delta} \quad (6-19)$$

electron-hole pairs.

On the other hand, the absorption coefficient of hard x-rays is small compared to the visible light, therefore the quantum efficiency is smaller. To compensate for weaker absorption, the thickness of the active (depletion) region is increased (up to several cm, Figure 71). In order to effectively collect the charge over such a wide depletion region, a large reverse bias voltage (\sim kV) is applied.

Semiconductor detectors can be operated in the *pulse mode* in the x-ray energy range and the pulse height can be used for particle energy measurements, just as in the case of gas proportional counters or scintillator detectors.

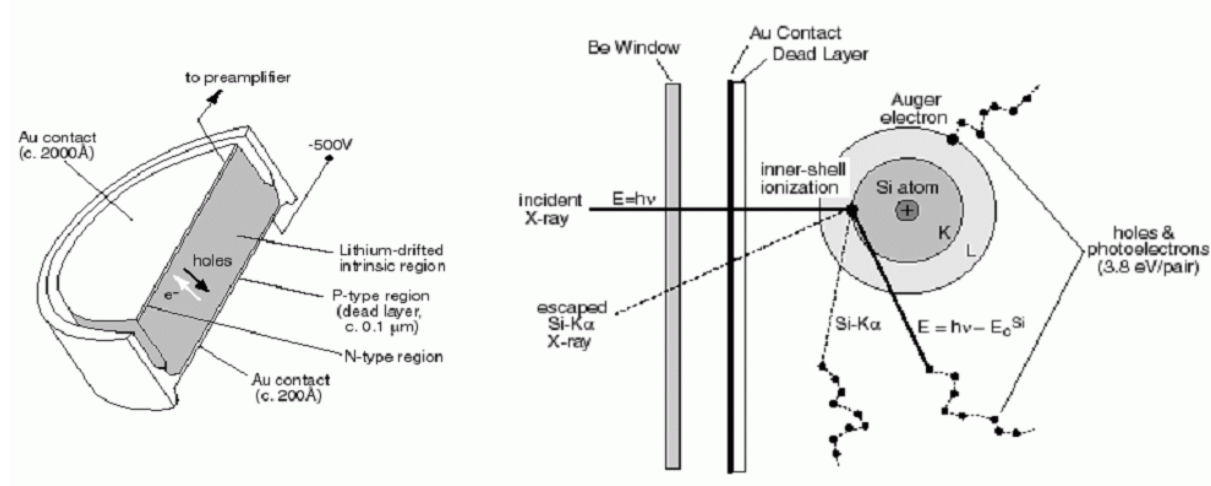


Figure 71. (Left) A cross-section of an x-ray detector, **(right)** x-ray induced processes.

The majority of x-ray and gamma detectors are silicon- or germanium-based:

Si(Li) detector

A lithium-drifted Si(Li) detector is manufactured from high-purity p-type silica. However, p-type silica of sufficiently high purity is difficult to fabricate. Most Si crystals contain extrinsic holes, caused by impurities, which allow significant "leakage" of current at the required bias voltage. In order to compensate for these extrinsic holes, lithium, an n-type dopant, is diffused into the material at 350 - 450°C under an electrical gradient. The lithium atoms compensate for the extrinsic charge-carriers in the p-type silicon and provide a wide "intrinsic" region of high resistance. Si(Li) detectors are operated at 77 K with a liquid N₂ cryostat to prevent further diffusion and to reduce the level of random noise due to the thermal motion of charge carriers.

Si is widely used in the wavelength range from 1 keV to 50 keV. Due to its low atomic number, the absorption cross-section for even higher-energy radiation becomes too small.

Ge(Li) detector

This is the most popular early detector types. Ge has higher atomic number and has therefore better sensitivity to high-energy gamma rays. It is also technically possible to manufacture wider intrinsic regions in Ge than in Si, so that Ge detectors can be used for radiation of a few MeV energy. Compared to Si, the band gap and the pair creation energy is smaller (Figure 70), so that \bar{n} (6-19) is higher and also the Fano factor is smaller in Ge (0.08) than in Li (0.1), which both contribute to give $\sim 27\%$ better energy resolution in Ge. However, the narrower band-gap also increases the number of thermally created electron-hole pairs and therefore the background (dark) current in the detector. The Ge detectors should be cooled to liquid nitrogen temperatures to produce spectroscopic data.

High-purity Ge (HPGe) detector

As the technology advanced, it became possible to manufacture Ge crystals with so high purity, that the Li-doping for counterbalancing the effect of impurities became obsolete.

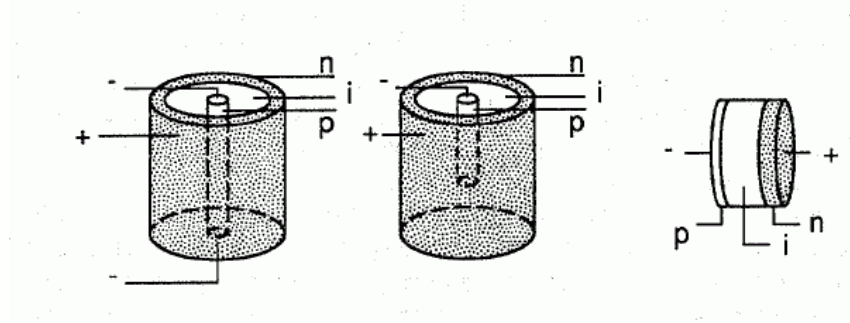


Figure 72. Solid state x-ray detector configurations: coaxial, close-ended cylindrical and planar.

Table 5. Properties of x-ray detector materials.

Property	Si	Ge	GaAs	Diamond
Atomic Number	14	32	31/33	6
Atomic Mass [amu]	28.1	72.6	144.6	12.6
Band Gap [eV]	1.12	0.66	1.42	5.5
Radiation Length X_0 [cm]	9.4	2.3	2.3	18.8
Average Energy for Creation of an Electron-Hole Pair [eV]	3.6	2.9	4.1	~ 13
Average Energy Loss dE/dx [MeV/cm]	3.9	7.5	7.7	3.8
Average Signal [$e^-/\mu m$]	110	260	173	~ 50
Intrinsic Charge Carrier Concentration [cm^{-3}]	$1.5 \cdot 10^{10}$	$2.4 \cdot 10^{13}$	$1.8 \cdot 10^6$	$< 10^3$
Electron Mobility [cm^2/Vs]	1500	3900	8500	1800
Hole Mobility [cm^2/Vs]	450	1900	400	1200

6.7 Time response

The equivalent circuit of a semiconductor detector operated as a spectrometer is shown in Figure 73. If a zero-electric-field radiation-insensitive region is present in the detector, its resistance appears in series with the circuit and is indicated in Figure 73 by R_d . Other electrical characteristics of the detector itself are C_d – the capacitance and R_p – the resistance of the depletion region (in most cases, effects of high resistance of the reverse-biased junction are negligible.) The creation of the charge carriers and their drift to the electrodes is represented by the current generator $I(t)$.

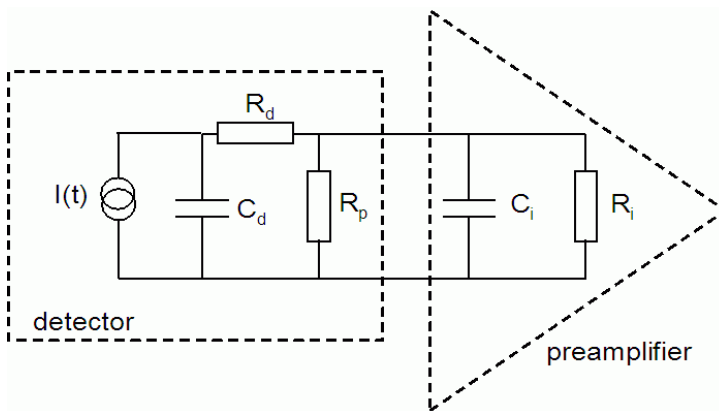


Figure 73. Equivalent circuit of semiconductor detector.

When semiconductor detectors are used for particle energy measurement, they are normally connected to a charge-sensitive (integrating) preamplifier with a high dynamic input capacitance. The charge-sensitive preamplifier integrates on its feedback capacitance the current signal delivered by the detector and feeds the resulting voltage signal to the filter amplifier (main amplifier). The time behavior of the current signal at the input of the charge-sensitive preamplifier is determined by the current signal's shape and by the effect of the equivalent circuit shown in Figure 73. The effect of the equivalent circuit is usually easily calculated, whereas detailed considerations on the charge collection process in the detector are needed to calculate the temporal properties of the induced current signal $I(t)$.

As in gas-filled detectors, the pulse formation can be thought of as a combination of the motion of electrons and holes. The charge collection time is given by the drift velocity of the corresponding carriers and the thickness of the depletion layer. The drift velocity of holes is ≈ 3 times slower than that of electrons in a semiconductor. The complete charge collection time t_c is given by the worst case: a hole traveling across the entire depletion layer thickness. The time is given by the thickness divided by the hole drift velocity. t_c ranges from $<1\text{ns}$ to about 100ns .

The **shape of the pulse** of a diode is determined by these factors:

- 1) The charge collection time t_c .
- 2) The resistance and capacitance present in the detector and measuring circuitry and the charge carrier transit time. Capacitance C_d of the diode is given by the material's permittivity ϵ , area A , and thickness of the depletion region D :

$$C_d = \epsilon \frac{A}{D} \quad (6-20)$$

Typically, C_d is several pF. The diode's series resistance R_d is mainly governed by the distance electrons need to travel in the field free n-region towards the n+ electrode. It ranges from a few ohms to tens to ohms. The minimum of the rise time set by the RC-circuit can be <1ns for fast photodiodes.

- 3) The variation of the position of absorption within the depletion region and the variation of the drift velocities. It should be also noted that carrier motion by diffusion is a much slower process than the motion by drift. When a high speed photodiode is fully exposed to radiation, carriers are also generated at the diode periphery. These carriers are collected by diffusion process because of absence of the electric field in this region. This can result in the diode fall time much higher than the risetime.
- 4) Plasma effects. Particularly in charged particle detection, a particle first produces a dense cloud of electron-hole pairs, into which the electric field cannot penetrate. Only after the cloud has sufficiently diffused can the bias voltage penetrate it and the carriers begin to drift towards the electrodes. This creates a delay in the detected pulse.

6.7.1 Trapping effects:

Trapping of a charge carrier in a semiconductor occurs when the carrier is captured by an impurity or imperfection center and is temporarily lost to any charge transport process. In semiconductor detectors, it is useful to introduce the quantity τ_{drift} (mean free drift time):

$$\tau_{drift} = \frac{1}{N_t \sigma v} \quad (6-21)$$

where N_t is the density of trapping centers, σ the trapping cross section and v the velocity of carriers. The trapped charge carrier can be reemitted in the relevant band and take part again in the charge transport process. The average time spent by a carrier in a trap is called the *mean detrapping time* τ_D and is strongly temperature dependent:

$$\tau_D \sim \exp\left(\frac{E_\tau}{kT}\right) \quad (6-22)$$

where E_τ = activation energy of the trap, k = Boltzmann's constant, T = absolute temperature.

If the mean detrapping time is of the same order of magnitude as, or larger than, the electronic shaping constants, the charge carrier is lost to the charge collection process or is collected with significantly reduced efficiency. The result is poor energy resolution and peak tailing. On the other hand, if the mean detrapping time is orders of magnitude shorter than the charge collection time due to drift of the carriers, then the trap has no effect on the charge collection process. For this reason, normally used dopants such as Li, P, B, and Ga, which are shallow donors or acceptors, do not act as traps.

It can be shown that to first-order approximation, the efficiency of collection of a charge carrier subjected to trapping with a mean free drift time τ_{drift} is given by

$$\eta = 1 - \frac{t_c}{2\tau_{drift}} \quad (6-23)$$

where t_c is the charge collection time.

In a modern germanium gamma-ray spectrometer the charge collection efficiency is of the order of 0.999, and as t_c is of the order of 10^{-7} s, then τ_{drift} , according to Eq.(6-23), is of the order of 10^{-4} s.

In Ge detectors, the typical values of v and σ are 10^7 cm · s⁻¹ and 10^{-13} cm² respectively, the maximum concentration of trapping centers permissible in the detector is of the order of 10^{10} cm⁻³, corresponding to approximately 1 for every 10^{12} atoms of germanium.

6.8 Radiation damage

Semiconductor detectors used for x-rays, gamma-rays or energetic charged particles, are susceptible of radiation damage, which results in the degradation of the detector's performance over time. There are two basic radiation damage mechanisms:

- ***Displacements.*** These are dislocations of atoms from their normal sites in the lattice, producing less ordered structures, with long term effects on semiconductor properties.
- ***Long term ionization.*** In insulators, the material does not return to its initial state, if the electrons and holes produced are fixed, and charged regions are induced.

Displacements determine the degradation of the bulk, and long term ionization is responsible for surface damage.

Producing displacements is a four-step process:

- The primary particle hits an atom in the lattice, transferring enough energy to displace it. In the case of high energies, nuclear reactions can occur, producing several fragments or secondary particles.
- The fragments of the target atom migrate through the lattice causing further displacements. The mean free path between two successive collisions decreases towards the end of the range, so that defects produced are close enough and can interact.
- Thermally activated motion causes rearrangement of the lattice defects at room temperature (*annealing*).
- Thermally stable defects influence the semiconductor properties, i.e. the detector parameters.

Effects of displacements are:

- Change of effective doping concentration (higher depletion voltage, under- depletion).
- Increase of leakage current (increase of shot noise, thermal runaway).
- Increase of charge carrier trapping (loss of charge).

Long term ionization effects also comprise several steps:

- Ionization is produced along the track of the primary ionizing particle, or sometimes in restricted regions around a nuclear reaction.
- Many of the e-h pairs produced recombine. The electrons which did not recombine in the initial phase diffuse or drift away. Some electrons end up on traps, others may escape from the insulator.
- The carriers trapped on levels with low ionization energies are thermally reexcited and get into the conduction or valence band; they are subject to further drift or diffusion, and leave the dielectric or are captured on deep trap levels (practically permanent).
- The net effect of the induced charges is the change of the electric field in the semiconductor, in the vicinity of the interface.

6.9 Energy resolution in pulse height spectroscopy

For several detector types (gas-filled proportional counter, scintillation, semiconductor), we considered the question of the energy resolution in pulse height spectroscopy. All these devices can be used to measure the energy (pulse height) spectrum of the absorbed radiation. A typical spectrum from a monoenergetic γ -ray source (^{137}Cs , $h\nu=661.6 \text{ keV}$) is shown in Figure 74.

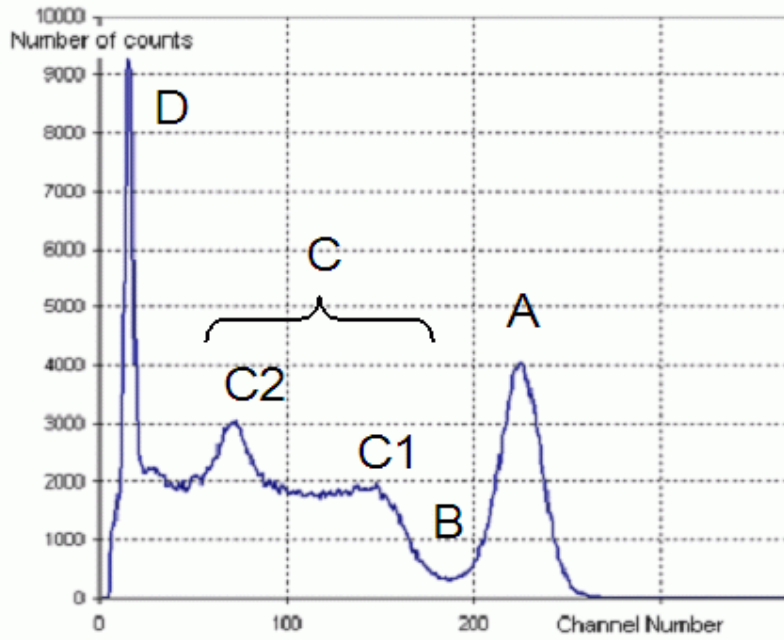


Figure 74. A pulse height spectrum of Cs-137 radiation, measured with NaI scintillation detector.

The spectrum shows the characteristic regions that are common regardless of the detector type used:

- A** Photopeak, from the absorption of the γ -quantum in the NaI scintillator.
- B** “Compton valley”, only from multiple Compton scattering events.
- C** Compton scattering, partial energy loss by the γ -quantum.
- C1** Compton edge, maximum possible energy loss by the γ -quantum by Compton scattering – a “head-on” collision with an electron, scattering angle 180 deg.
- C2** Backscatter peak, Compton scattering in one of the materials surrounding detector.
- D** Electronic noise.

The statistical component of the detector’s resolution R is limited by the average number \bar{n} of charge carriers liberated by one incoming particle, since (see Eq. (2-26))

$$R \sim \bar{n}^{-\frac{1}{2}} \quad (6-24)$$

Inherently, semiconductor detectors offer considerably better resolution, since their mean pair-creation energy is smaller than in gas-filled detectors ($\delta = 2.9$ eV (Ge), 3.6 eV (Si), compared to 26 eV in Ar and to 25 eV, which is the mean energy required to produce a fluorescence photon in NaI). In addition, the resolution is improved by the smaller Fano factor in semiconductors than in scintillators. A direct comparison between different detector types is given in Figure 75.

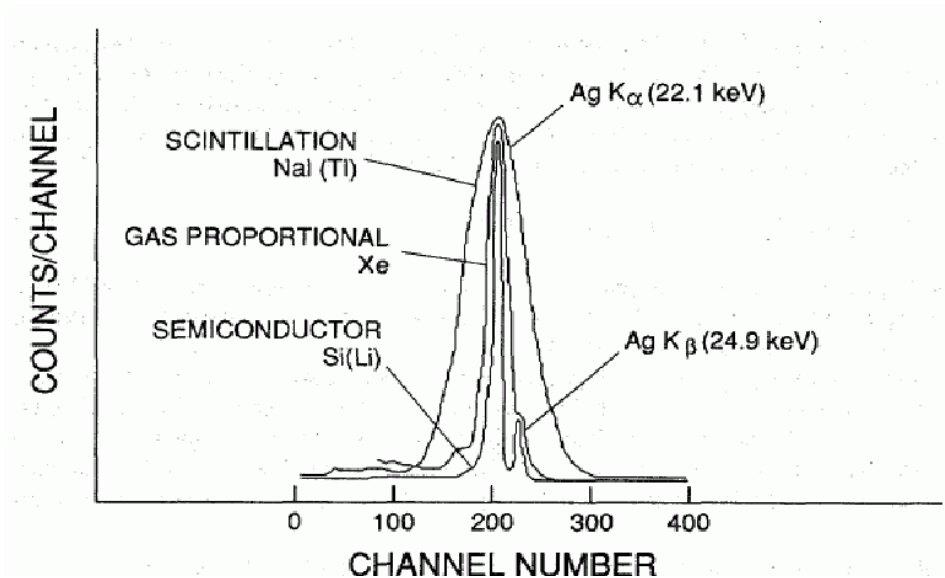


Figure 75. The photopeak of Ag K α radiation by different detectors [H.A. Smith and M. Lucas, *Gamma-ray detectors*].

The advantages of better energy resolution are best illustrated by the case of a non-monochromatic source, with several close-lying photopeaks (Figure 76).

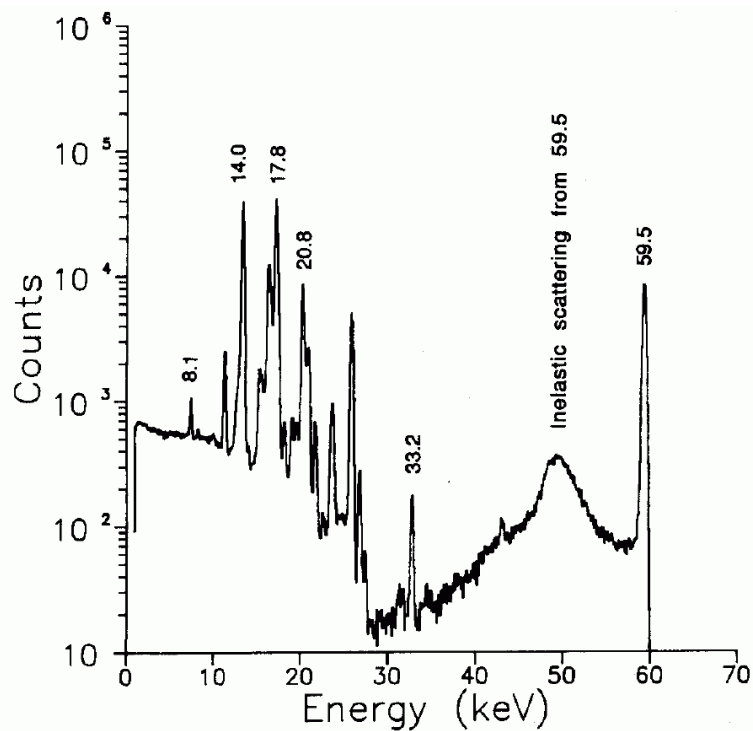


Figure 76. Am-241 spectrum measured by Si(Li) detector [C.S. Rossington et al, IEEE Transactions of Nuclear Science, vol. 39, p- 570 (1992)]

7 Other devices

7.1 Charge-coupled devices (CCDs) and image intensifiers

The CCD devices are semiconductor detectors, primarily for visible light. Invented in the late 1960s by researchers at Bell Labs, it was initially conceived of as a new type of computer memory circuit. It soon became apparent that the CCD had many other potential applications, including signal processing and imaging. The CCD's early promise as a memory element has since disappeared, but its superb ability to detect light has turned it into the industry-standard image sensor technology.

CCD imaging is performed in a three-step process:

1. Exposure – creation and trapping of electron-hole pairs
2. Charge transfer – moves the packets of charge within the silicon substrate
3. Charge-to-voltage conversion and output amplification.

CCDs follow the principles of basic metal oxide semiconductor (MOS) device physics. The basic element is a MOS-capacitor. This serves both to store photoelectrons and to shift them. CCD consists of a transparent metal electrode separated by a $\sim 0.1\mu\text{m}$ of SiO_2 insulator from a layer of p-type Si (Figure 77), thus it is a simple capacitor. The bulk material is p-silicon, that can be made to have very small numbers of free electrons ("high resistivity") before exposure to light; this is important for best performance. A positive potential applied to the electrode repels the holes (majority carriers in the p-type silicon) and forms a potential well at the silicon surface. This serves as one pixel, and is typically $10\text{-}20\mu\text{m}$ square.

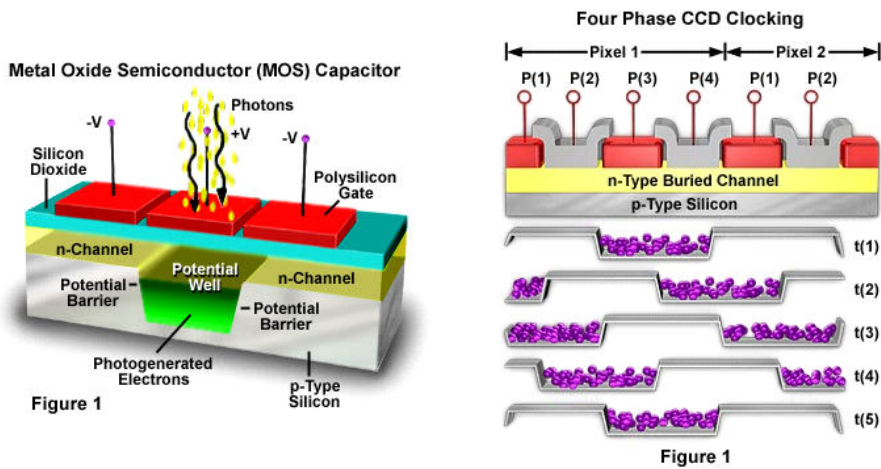


Figure 77. Left: CCD device. Right: transferring trapped charge.

Trapping charge: Before exposure, the central electrode is set to a positive bias while the two flanking electrodes are set negative. This creates a depletion region under the central electrode containing no holes but a deep potential well to trap electrons. If a photon with sufficient energy is absorbed into the depletion region, it forms an electron-hole pair which splits as the electron is attracted to the positive electrode. In this way, minority carriers (electrons) accumulate at the oxide semiconductor interface in an inversion layer about 10nm thick.

An image is acquired when the array of pixels is illuminated, creating electron-hole pairs. The collected charge is linearly dependent on the light intensity and exposure time. Charge (electrons) is collected in potential wells created by applying a voltage to the polysilicon (gate) electrode. Practical potential-well capacities range up to a 10^6 electrons, with depletion depths from 6 to 30 μm and more.

Transferring charge: After exposure, the individual charge pockets must be moved to the electrodes and measured. It is done by changing the polarity of the gates in sequence, moving the potential wells and charge packets along the chain. In a four-phase CCD, four gates are used to define each pixel (Figure 77). The packets of charge are eventually shifted to the output sense node, creating a voltage on the electrodes. Another option is the three-phase CCD, in which three out-of-phase clock voltages transfer the charge across the array (Figure 78):

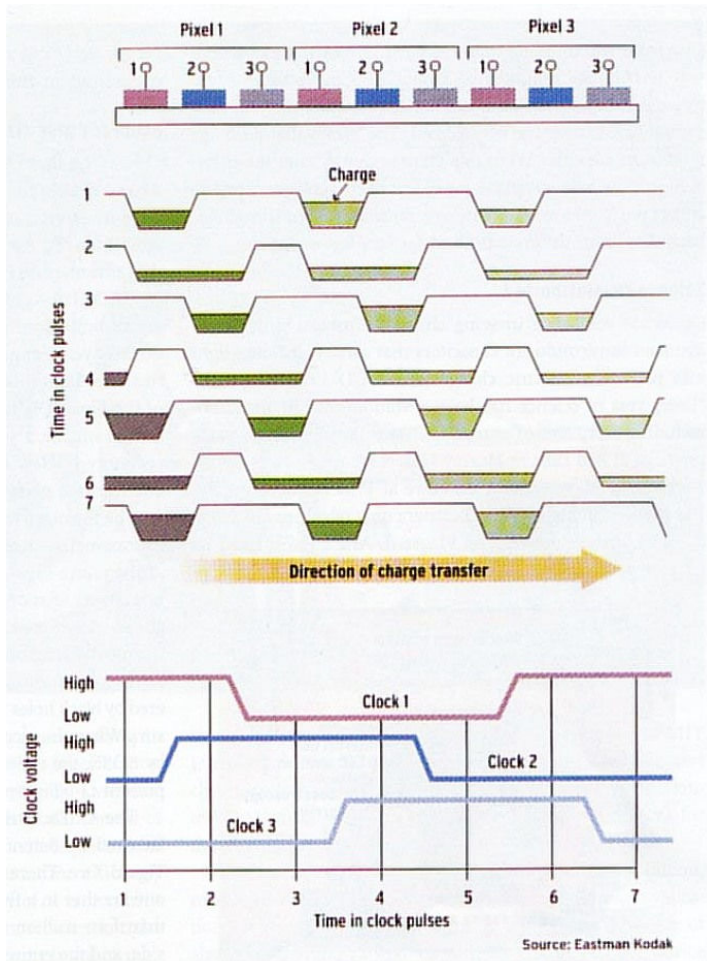


Figure 78. Reading out CCD cells by three-phase clocking.

Stage 1: Clock 1 is high and clocks 2 and 3 are low, so all the collected charge is held under the gates labelled 1.

Stage 2: Clock 1 and 2 are high and clock 3 is low, so the charge spreads out below gates 1 and 2.

Stage 3: Clock 3 is brought low so all of the charge shifts to under gate 2. The result is that the charge has been shifted to the right by one gate. This process is repeated many times until all of the charge is transferred out of the CCD to a collecting electrode and into an output amplifier.

The CCD device has high quantum efficiency (about 80%) for the visible light, but low gain (only one electron-hole pair is created per photon). The MCP, on the other hand, can have very high gains (10^6) and has low noise. The two sensors are combined in the 2nd generation **image intensifiers** (or 3rd generation if using the GaAs photocathodes), used for example in night vision goggles. As seen in Fig. 5-11, the image is first projected onto a photocathode, where photoemission of an electron occurs. Under HV bias, the electron is multiplied by the MCP and the cascade of secondary

electrons hits a fluorescent material, where a flash of light is created. Finally, the image can be read out by a CCD device.

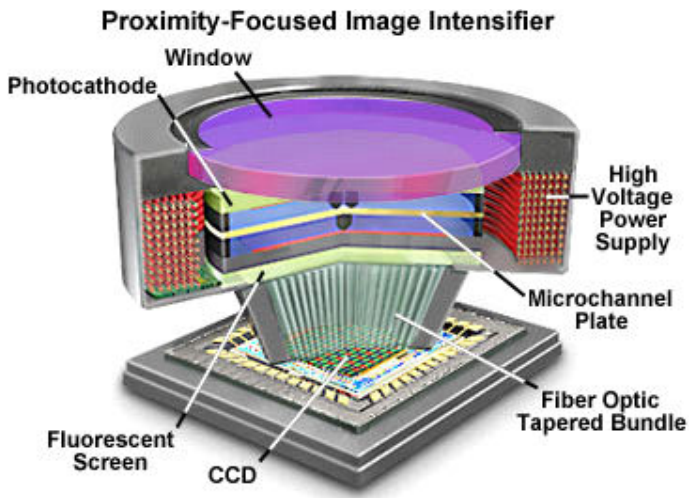


Figure 79. Image intensifier design, based on MCP and CCD detectors.

7.2 Photochemical sensors (human eye)

The energy provided by the absorbed light can also initiate chemical reactions or changes in the molecular geometry. This is the basis of the operation of human eye. In the human eye, light is registered on the *retina*, a thin film of tissue which covers the interior of the eye behind the lens. The retina contains photosensitive cells known as *rods* and *cones*. Rod cells are used in dim light, and produce only black and white images. Cone cells operate in bright light and produce the colors we perceive. Within each rod cell are about 1000 disks containing the protein *rhodopsin* - made from 11-cis-retinal (vitamin A) attaching to opsin.

When light is absorbed by rhodopsin, the double bond electrons are promoted to a π^* orbital, which allows the bond to freely rotate and the molecule is converted into trans-retinal. The trans-retinal is bleached and cannot respond to more light until it isomerizes back to the cis- form and attaches to the protein opsin again. Thus a complex chemical reaction known as the **rhodopsin cycle** takes

place every time a photo receptor cell is stimulated by light of the correct frequency.

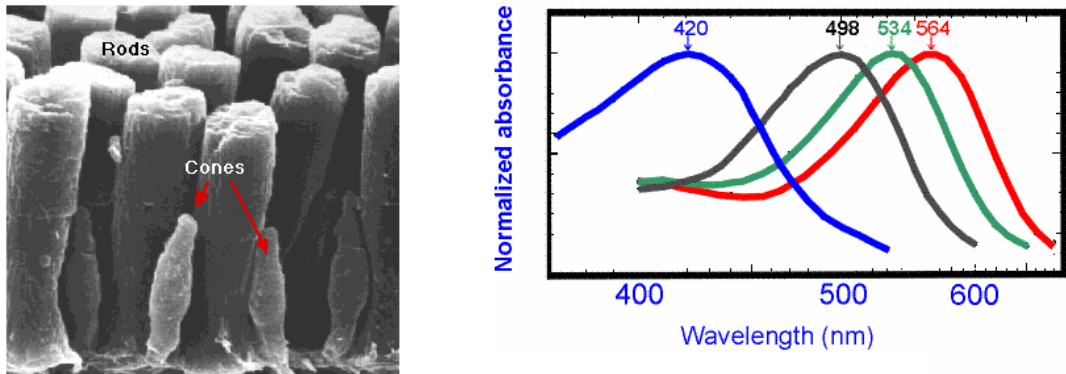


Figure 80. Left: Microscopic image of the sensors in the human eye. **Right:** Spectral sensitivity of the different receptors (blue, green, red – cones, black – rods).

Within the cells a cyclic metabolic pathway regenerates the pigment, produces more or less of it as needed to adapt to light conditions, and permits constant response. The first response to light is, then, a physiochemical phenomenon, which ultimately leads to an alteration in the surface charge of the light sensitive cell. This in turn is translated into nervous signals and action potentials.

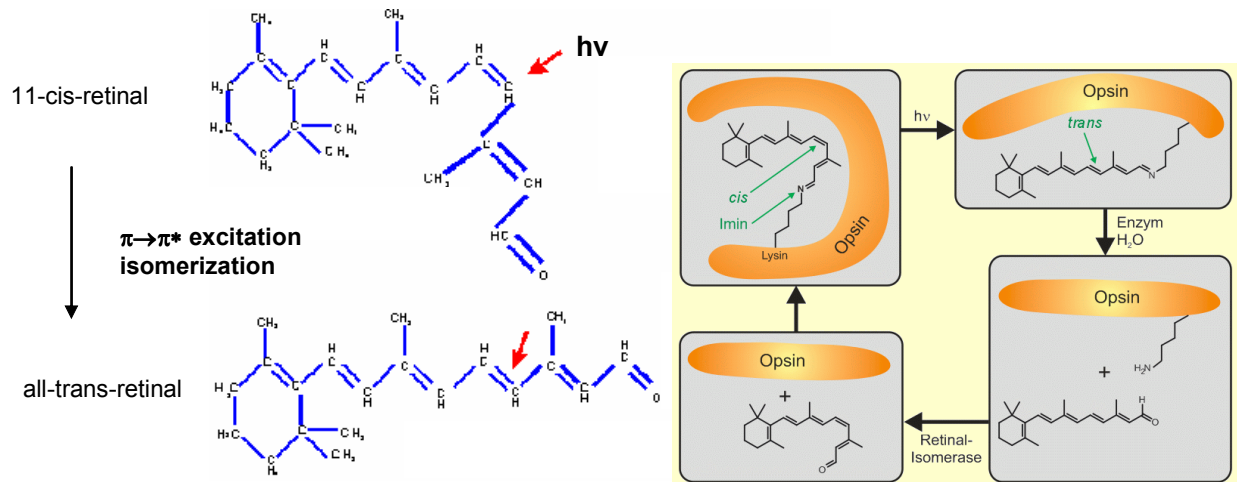


Figure 81. Left: Isomerization. **Right:** Outline of the Rhodopsin cycle.

The hyperpolarization response to the absorption of light is proportional to light intensity; and thus the brighter the illumination the greater the hyperpolarization. The net change in overall membrane charge is perceived by the integrating neurons of the retina. They in turn pass the information (with suitable inhibitory and/or excitatory signals of their own) to the ganglion cells. Ganglion cells send their axons out via the optic nerves and into the visual processing centers of the central nervous system.

The light level striking the rod is thus translated first into a cascade of chemical changes via the rhodopsin cycle, and ultimately into modification of electrical potential, making the transduction of the electromagnetic energy to neuronal signal. The process of color vision involves cones, but the mechanism (absorption of energy, hyperpolarization of the cone surface membrane, and detection by bipolar and horizontal cells) is identical.

Table of Contents

1	INTRODUCTION	3
2	INTERACTION OF PARTICLES AND RADIATION WITH MATTER	5
2.1	Radiation	5
2.1.1	Photoelectric effect.....	5
2.1.2	Other processes.....	8
2.2	Electrons and ions	9
2.3	Neutrons	11
2.4	Relaxation processes.....	12
3	UNITS AND DETECTOR CHARACTERISTICS	14
3.1	Useful units.....	14
3.2	Common detector characteristics.....	15
3.2.1	Temporal properties.....	15
3.2.2	Statistical properties	17
3.2.3	Other properties	20
4	GAS-FILLED DETECTORS	22
4.1	Electrons and ions in gases	22
4.1.1	Motion of free charges.....	22
4.1.2	Recombination and capture	25
4.2	Operational regions	25
4.3	Avalance ionization	30
4.4	Pulse formation in an ionization chamber.....	32
4.5	X-ray imaging in a multiwire chamber	34
4.6	Gas electron mulitplier (GEM)	36
4.7	Detection of neutrons	36
5	SURFACE PHOTOEMISSION DETECTORS	38
5.1	Photocathodes and Phototubes	38
5.2	Photomultiplier tubes.....	41
5.2.1	Principle.....	41
5.2.2	Electron-Optical Input System.....	44
5.2.3	Gain	44
5.2.4	Time structure.....	46
5.2.5	Noise	47
5.2.6	Current and pulse mode operation	48
5.3	Channeltrons.....	50
5.4	Microchannel plates	51
5.5	Scintillation detectors.....	52
5.6	Position sensivite detection with MCPs	54
6	SEMICONDUCTOR DETECTORS	56

6.1	Band structure concepts.....	56
6.1.1	Electrons and holes.....	56
6.1.2	Direct and indirect band gap.....	57
6.1.3	Effective mass.....	59
6.2	Intrinsic and doped semiconductors	59
6.3	p-n junctions	60
6.3.1	Biased p-n junctions	63
6.4	Photodiodes and solar cells.....	65
6.4.1	Generating photocurrent	65
6.5	Visible and infrared light detectors	69
6.5.1	Absorption and spectral responsivity.....	69
6.5.2	Light detector types	71
6.6	Semiconductor γ- and x-ray detectors	74
6.7	Time response	77
6.7.1	Trapping effects:.....	78
6.8	Radiation damage.....	79
6.9	Energy resolution in pulse height spectroscopy	80
7	OTHER DEVICES	83
7.1	Charge-coupled devices (CCDs) and image intensifiers	83
7.2	Photochemical sensors (human eye)	86
Table of Contents.....		89